Food Packaging and Shelf Life 37 (2023) 101096

Contents lists available at ScienceDirect

Food Packaging and Shelf Life

journal homepage: www.elsevier.com/locate/fpsl

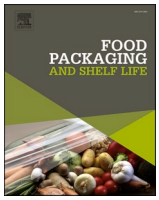

Tailor-made coextruded blown films based on biodegradable blends for hot filling and frozen food packaging

Annalisa Apicella, Paola Scarfato *, Loredana Incarnato

Department of Industrial Engineering, University of Salerno, Via Giovanni Paolo II, 132, 84084 Fisciano, SA, Italy

ARTICLE INFO

Keywords:
Multifunctional biodegradable film
PBS/PLA
PBAT/PLA
Coextruded blown films
Hot filling
Film for frozen foods

ABSTRACT

Biodegradable polymers still have severe limitations in their application over wide temperature ranges. In this study, we developed coextruded bilayer biodegradable packaging suitable for either hot-filling and frozen food products. The films were realized by combining an inner layer, made of Ecovio and amorphous poly(lactide) (PLA4060) blend, providing high ductility and sealability, with an outer layer made of poly(butylene succinate) (PBS) and semicrystalline PLA4032 blend, contributing to barrier properties and thermal resistance. The concentration of each blend was optimized for the target application based on preliminary chemical-physical investigations. Then, three bilayer structures with different relative thicknesses of the layers were realized and analyzed for their mechanical, barrier, wettability, sealability and overall migration properties in the −18÷85 °C temperature range, to check their compliance with the needs of food packaging applications involving both thermal treatment and freezing. The coextruded films had functional performance generally intermediate those of the single layers and weighted on their relative thicknesses, and overall migration values complying the limits of Regulation (EU) No 10/2011 for plastic packaging intended for both hot filling process and long-term frozen food storage. Among all, the most suitable structure for the target application was the bilayer film with the largest thickness of the outer layer (i.e. 50 μm), which showed the best balance between stiffness and ductility in the explored temperature range. In particular, it displayed the lowest lowering of elastic modulus at 85 °C, which becomes equal to 135 MPa, and an elongation at break equal to 40 % at −18 °C.

1. Introduction

Replacing fossil-derived plastics with biodegradable polymers was recently identified by academic and industrial research as a challenging solution to reduce terrestrial and marine ecosystems pollution and to achieve Sustainable Development Goals (Riechers et al., 2021; Kumar et al., 2021). The use of bioplastics in the packaging field accounted for almost 48 % (1.1 million tons) of the total market in 2022 (European Bioplastics, 2022). Despite the undoubted ecological advantages, the functional properties of biodegradable polymers are in most cases inferior to those of conventional fossil-based materials and are not entirely satisfactory for the food and beverage market, which requires high-performance technologies and materials customized to the individual requirements of each food product and at low cost (Apicella, Scarfato, Di Maio, & Incarnato, 2018; Leneveu-Jenvrin et al., 2021; Jeong, Lee, Cho, & Yoo, 2020; Li, Qin, Liu, Li, & Zhong, 2022; Grzebieniarz, Biswas, Roy, & Jamróz, 2023; Ouahioune et al., 2022; Apicella & Carlucci, 2022).

In the food industry, for instance, a considerable amount of foods undergoes pasteurization and hot-fill processes at relatively high temperatures (85 °C or higher) with the aim of reducing the microorganisms concentration to safe limits and of inactivating enzymes inducing browning and fermentation phenomena. (Johnson, 2018). During this step, the inner surfaces of the packaging are also subjected to heat treatment for a short time in order to ensure their pasteurization (Rahman, 2011). This implies, therefore, that the material used must be heat-resistant in order to keep intact its structural and barrier performance even after exposure to high temperatures (Adegoke, 2004). Further complicating the scenario is the fact that some of these products (e.g., fruit juice popsicles, frozen desserts, sauces, and dairy products), after the hot-filling stage, require refrigerated or freezer storage, so it is critical that the packaging material maintains good performance even at low temperatures (Pietrosanto, Scarfato, Di Maio, Nobile, & Incarnato, 2020). Special multilayer films consisting of an inner heat sealable layer (generally made of polypropylene or polyethylene) a barrier layer (made of metal oxide-coated polyethylene terephthalate, ethylene vinyl

* Corresponding author.
E-mail address: pscarfato@unisa.it (P. Scarfato).

https://doi.org/10.1016/j.fpsl.2023.101096
Received 15 February 2023; Received in revised form 22 May 2023; Accepted 7 June 2023
Available online 14 June 2023

alcohol or nylon) and of an outer layer providing heat-stability, water-resistance and printability (polyethylene terephthalate/ polyethylene) are generally employed for these applications (Sonar, Tang, & Sablani, 2022). As is evident, the composition of these structures, whether coextruded or laminated, is neither recyclable nor biodegradable after use, nor are monolayer films commonly used because of the limitations of each polymer. Finding sustainable alternatives is therefore a priority, although not an easy task.

Within the global bioplastics throughput, poly(butylene adipate-co-terephthalate) (PBAT), polylactide (PLA) and poly(butylene succinate) (PBS) now make up 19.2 %, 18.9 % and 3.5 %, respectively (European Bioplastics, 2022). PLA is usually designated as the favorite bio-polymer for applications in the food packaging field, due to its satisfactory mechanical strength, processability and optical properties, as well as printability and heat-sealability (for amorphous grades). Nevertheless, its scarce heat resistance, gas barrier properties and inherent fragility hardly limit its large-scale application in the food packaging field (Vorawongsagul, Pratumpong, & Pechyen, 2021; Piscopo et al., 2019; Chen et al., 2022). On its turn, PBS shows satisfactory toughness and impact resistance, coupled to good thermal and chemical resistance; moreover, its high flexibility makes it suitable for applications involving blown film production. However, it is poorly heat-weldable, and this constraints its use as a packaging material. (Aliotta, Seggiani, Lazzeri, Gigante, & Cinelli, 2022). Lastly, PBAT is recognized as an extremely ductile and flexible material even at low temperatures, but its poor barrier, optical and sealing performance has limited its use to date (Pietrosanto et al., 2020; Su, Duhme, & Kopitzky, 2020).

Melt blending, as well as multi-layer co-extrusion, are among the most effective strategies to combine the functional performances of single biopolymers, overcoming their drawbacks and expanding their commercial uptake in the packaging field (Scaffaro, Maio, Gulino, Di Salvo, & Arcarisi, 2020; Ahmed, Mulla, Al-Zuwayed, Joseph, & Auras, 2022). These two technologies are of relevance for manufacturing of packaging films on an industrial large scale; combining the two technologies together, in particular, enables the realization of multifunctional materials whose properties can be tailored, optimized and engineered on demand.

Although PLA is not miscible with either PBS or PBAT, it is known that their blending allows to improve material performance. As for films based on PLA/PBS blends, several authors have reported the enhancement of impact strength (Ostrowska, Sadurski, Paluch, Tyński, & Bogusz, 2019), flexibility and elongation at break (Chen & Yoon, 2005; Gigante & Coltelli, 2019), the improvement of PLA crystallization behaviour (Ostrowska et al., 2019; Homklin & Hongsriphan, 2013; Qiu, Song, & Zhao, 2016; Wang, Wang, Zhang, Wan, & Ma, 2009; Yokohara & Yamaguchi, 2008) as well as higher biocompatibility (Gigante & Coltelli, 2019) and accelerated hydrolytic degradation (Wang Y.P., 2016).

Regarding films based on PLA/PBAT blends, researchers have reported significant improvements in processability for film blowing and ductility already at low ($\leq$ 20 wt. %) PBAT concentrations, although at the detriment of films stiffness (Pietrosanto, Apicella, Scarfato, Incarnato, & Di Maio, 2022; Hongdilokkul et al., 2015; Wang, Peng, Chen, Yu, & Zhao, 2019; Li X., 2018; Andrade et al., 2022). Some recent researches have also emphasized the suitability of these structures for refrigerated and frozen food packaging applications (Gigante, Canesi et al., 2019; Pietrosanto et al., 2020). Very few articles, however, address the application or modification of PLA/PBAT blends available on the market, such as Ecovio ® (Facchi, Souza, Almeida, Bonafé, & Martins, 2021; Mohr et al., 2019; Signori et al., 2015).

As regards multilayer biodegradable films, previous literature focused on the melt coextrusion of pure PLA/PBS (Scaffaro et al., 2020; Messin et al., 2020), PLA/PHBV (Boufarguine, Guinault, Miquelard-Garnier, & Sollogoub, 2013), PHBV/PBAT (Cunha, Fernandes, Covas, Vicente, & Hilliou, 2016), PHA/PVOH/PHA (Thellen, Cheney, & Ratto, 2013), or nanocomposites, such as PLA/PLA-graphene (Li C., 2018), PLA/PLA-layered silicate/PLA (Scarfato et al., 2017). To our best knowledge, almost no work in literature reports the realization of coextruded films based on biodegradable blends. Moreover, this is the first study in which multilayer films based on tailor-made biodegradable blends are realized with the aim of gathering the performance of the components into an innovative packaging suitable for hot-filling and frozen food products.

Herein, bilayer coextruded blown films were realized as follows: the inner layer (I) was obtained by blending Ecovio® F2332, a commercial blend based on PBAT and PLA exhibiting high ductility even at low temperatures, with an amorphous grade of PLA improving heat sealability; the outer layer (O), contributing to barrier properties and thermal resistance, was obtained by blending PBS and a semicrystalline grade of PLA. Three different structures were realized changing the relative thicknesses of the two layers. Prior to making the bilayer structures, monolayer films based on the blends having different composition were produced and tested, to identify the optimal concentrations for the target application. Monolayer samples were analyzed by infrared spectroscopy (ATR FT-IR) and differential scanning calorimetry (DSC), to evaluate possible modifications in chemical and thermal properties due to polymer blending. The coextruded films were characterized for their surface wettability, O_2 and water vapor barrier, heat-sealability, overall migration and tensile behavior. In particular, with the aim of verifying the prospects of the realized structures as a biodegradable films suitable for hot-fill and frozen food applications, the effects of temperature in the range from −18–85 °C were evaluated on mechanical and transport properties.

2. Experimental

2.1. Materials

Ecovio® F2223 (density = 1.24–1.26 g/cm^3, T_{m1}=110–120 °C, T_{m2}=140–155) was supplied by BASF (Ludwigshafen, Germany). It has been developed for the conversion to flexible films using a blown film process; according to the information disclosed by the patents, it is mainly composed by Ecoflex® F (PBAT), as the continuous phase in the structure, and PLA. PLA 4060D (amorphous, D-isomer content = 12 wt. %, Mw ~190,000 g/mol, density = 1.24 g/cm^3) and PLA 4032D (semicrystalline, D-isomer content = 1.5 wt. %, Mw ~155 000 g/mol, density = 1.24 g/cm^3, T_m=155–170 °C) were supplied by NatureWorks™ (Minnetonka, MN, USA). BioPBS™ FZ91PM (density = 1.26 g/cm^3 T_m=115 °C) was supplied by Mitsubishi Chemical Co. (Tokyo, Japan). All biodegradable polymers are suitable for food contact in conformity with regulations established by U.S. Food and Drug Administration (FDA) and European Union (EU). They also comply with EN13432 and ASTM D 6400 standards, regarding compostability under controlled composting conditions.

2.2. Realization of the blends and of the monolayer films

Before processing, PLA, PBS and Ecovio granules were vacuum-dried at 70 °C for 14 h. Blends of PBS and PLA 4032D (100/0, 90/10, 80/20, 70/30, 0/100 by weight) and of Ecovio and PLA 4060D (100/0, 80/20, 70/30, 0/100 by weight) were realized in a co-rotating twin screw extruder (Collin ZK25, with screw diameter equal to 25 mm and L/D = 42), selecting a screw speed equal to 150 rpm, a temperature profile from 150 °C to 190 °C for PBS/PLA blends and from 140 °C to 190 °C for Ecovio/PLA blend. Monolayer films based on the blends were made by a Gimac film blowing unit equipped by a single screw extruder (D = 12 mm, L/D = 24), a blow film spiral mandrel die (having inner and outer diameter equal to 30 mm and 30.5 mm, respectively) and a take-up/cooling system. The extruder operated using the same temperature profiles as described above. The blow-up ratio (BUR) was fixed at 2.5 for all the films, while the collection speed was set at 3 m/min. The obtained samples had an average thickness of 50 ± 2 μm.

2.3. Realization of the coextruded blown films

The preliminary investigation on monolayer films properties, whose results are discussed in detail later in the article, allowed to select the optimal compositions of the blends for the realization of the multilayer films. In particular, PBS/PLA4032 70/30 blend was selected for the realization of the outer layer while the Ecovio/PLA4060 70/30 was selected for the realization of the inner layer. The coextruded blown films were prepared by using the same Gimac film blowing unit as described before, but equipped by two single screw extruders. Both the extruders operated with a temperature profile equal to 190–175–175–185 °C from the hopper to the die. Three bilayer films were realized by varying the screw speed of the two extruders, and therefore the mass flow rates, yielding to two different thicknesses (i.e. 30 and 50 μm) for the outer (O) and inner (I) layer, as displayed in Table 1.

2.4. Characterizations

The ATR-FTIR spectra of the single layer films were obtained with a Nicolet 600 FTIR spectrophotometer (Thermo Scientific, Waltham, USA). The spectra were acquired in the range 650–4000 cm^{-1}, with 2 cm^{-1} resolution and a scan number of 64. Omnic software was used for normalization and peaks integration.

Thermal analyses on the monolayer films were conducted using a Differential Scanning Calorimeter (DSC mod. 822, Mettler Toledo). The heating/cooling thermal cycle was set at a rate of 10 °C/min in the range from − 70–200 °C under a nitrogen gas flow (100 mL/min), in order to avoid degradation phenomena due to thermal oxidation.

Optical microscopy (OM) observations were performed by means of a Zeiss Axioskop microscope (Carl Zeiss Vision, Germany) on film sections cut normally to the extrusion direction by cryofracture of the film in liquid nitrogen.

Oxygen permeability analyses were carried out in triple by a GDP-C gas permeabilimeter (Brugger, Munich, Germany) at 23 °C, 0 % R.H. and with 80 mL/min oxygen flow rate, according to ASTM D1434–82 procedure. The permeability coefficients (P_{O2}) were gained by multiplying the obtained oxygen transmission rate values by the thickness (mm) of each film. For multilayer structures the oxygen permeability coefficients were further calculated considering the permeability coefficients of the monolayers and their thickness, according to the following equations (Apicella, Barbato et al., 2022):

$$\frac{x_{Coex}}{P_{Coex}} = \frac{x_O}{P_O} + \frac{x_I}{P_I} \quad (1)$$

$$\frac{1}{Q_{tot}} = \sum \frac{x_i}{P_i} = \frac{1}{Q_1} + \frac{1}{Q_2} + \ldots \quad (2)$$

Where x and P refer to the thickness and the permeability coefficient of each layer i, subscripts "O" and "I" stand for the outer and inner layer, respectively, and "Coex" for the coextruded structure.

As for bilayer films, oxygen barrier properties were investigated both on unprocessed samples and on films subjected to hot filling process.

Water vapor permeability measurements were carried out in triple by a 7002 WP-Permeation Analyzer (Systech Illinois, Princeton, NJ, USA) at 23 °C and 50 % R.H, according to ASTM F 1249–90 procedure. The water vapor permeability coefficients (P_{H2O}) were gained by multiplying the obtained water vapor transmission rate values by the thickness (mm) of each film.

Tensile tests were carried out on films with at least ten replicates by a CMT 4000 SANS testing machine (MTS, China) using a 100 N load cell, following the to ASTM D 882–91 procedure. Film specimens having rectangular geometry (12.7 ×80 mm^2) were extended along the machine direction at ambient temperature (25 °C) and at −18 °C and 85 °C, simulating the typical temperatures of home freezers and of pasteurized liquid foods during industrial hot-filling process, respectively. These two latter temperatures were achieved within a closed chamber equipped with a temperature controller (mod. WK650) and with a liquid N_2 vessel (for frozen temperature).

Dynamic thermomechanical analysis (DMA) of monolayer films PBS/PLA4032 70/30, Ecovio/PLA4060 70/30 and of the bilayer film Coex O50/I30 were carried out on a DMA 800 dynamic mechanical analyzer (Perkin Elmer, Waltham, USA) working in tensile mode. Each film sample (about 12 × 5.5 mm) was tested from −40–120 °C at a heating rate of 2 °C/min under a liquid nitrogen atmosphere and at a fixed frequency of 1 Hz. The storage modulus (E′) and loss factor (tan δ) were determined, and the glass transition temperature (Tg) was taken at the maximum of the tangent of the loss angle (tanδ).

Single-side global migration tests were conducted in triple using stainless steel migration cells. The inner layer Ecovio/PLA4060 70/30 of the Coex O30/I50 sample, taken as representative of all the coextruded films, was cut gaining 2.5 dm^2 surface area and put in contact with a known volume (equal to 200 mL) of each food simulant. Three food simulants were selected in accordance with Regulation (EU) No 10/2011 (European Commission, 2011), i.e., 3 % acetic acid, 20 % ethanol and 50 % ethanol in distilled water (simulants B, C and D1, respectively). Contact tests were performed for 10 days at 40 °C (OM2). According to the Regulation (EU) No 10/2011, these standardized test conditions are suitable to simulate any long-term storage at room temperature or below, including heating up to 70 °C for up to 2 h or heating up to 100 °C for up to 15 min. Therefore, they are suitable for food packaging undergoing both hot filling process and frozen storage. After, the films were removed and the extracted solutions were transferred to quartz evaporation capsules and concentrated on a hot plate. The concentrated solutions were further evaporated to dryness at 100 ± 5 °C for 30 min, then cooled for 30 min in a desiccator and weighted. These steps were rerun till a constant weight of the residue was reached, to the nearest 0.1 mg. The conventional EU surface/volume ratio equal to 6 dm^2/kg food (6 dm^2/L simulant) was used for the calculation of the migration results.

Hot-tack tests were made to investigate the hot seal strength of the films in the temperature range 80–100 °C, by using a HSG-C heat seal tester (Brugger, Germany), according to ASTM F1921–98, Method B procedure. The selected temperatures correspond to the initiation sealing temperature and the one above which the film undergoes excessive warping and contraction, respectively. The welds were carried out on 15 mm-width samples, with 0.5 N/mm^2 sealing pressure and 1 s welding time.

Static contact angle measurements with the sessile drop method were recorded and analyzed at room temperature by a FTA 1000 Analyzer (First Ten Angstroms, Inc., Portsmouth, VA, USA) according to the ASTM D 7490 standard. A drop of 2 ± 0.5 μL volume was deposited on the sample surface through a syringe. The drop image was taken immediately after deposition by a video camera, and the contact angle was calculated from the drop shape through the proprietary image analysis

Table 1
Coextruded films nomenclature, nominal thicknesses of the outer (O) and inner (I) layers and screw speed of the extruders.

Sample	Total thickness [μm]	Outer layer [μm]	Inner layer [μm]	Extruder Screw speed [rpm]	
				Outer layer	Inner layer
O: PBS/PLA4032 70/30	50 ± 2	-	-	90	-
I: Ecovio/PLA4060 70/30	50 ± 2	-	-	-	90
Coex O30/I30	60 ± 3	30	30	55	55
Coex O50/I30	80 ± 5	50	30	95	55
Coex O30/I50	80 ± 5	30	50	55	95

software. Reported contact angles are the average of at least ten replicate measurements. Owens–Wendt (OW) geometric mean equation was applied to calculate the surface free energies (SFEs) of the inner and outer layer surfaces of the multilayer films, as well as the relative dispersive (γ_s^d) and polar (γ_s^p) components. (Owens & Wendt, 1969). Diiodomethane (DM) and distilled water (H_2O), having known SE values (Zonder, McCarthy, Rios, Ophir, & Kenig, 2014), were employed as testing liquids. The OW approach was also employed to calculate the work of adhesion W_a, in order to evaluate the quality of the interlayer adhesion of the coextruded films. In particular, the following set of equations was used (Apicella & Carlucci, 2022; Ebnesajjad & Landrock, 2015):

$$W_a = \gamma_S + \gamma_L - \gamma_{SL} \tag{3}$$

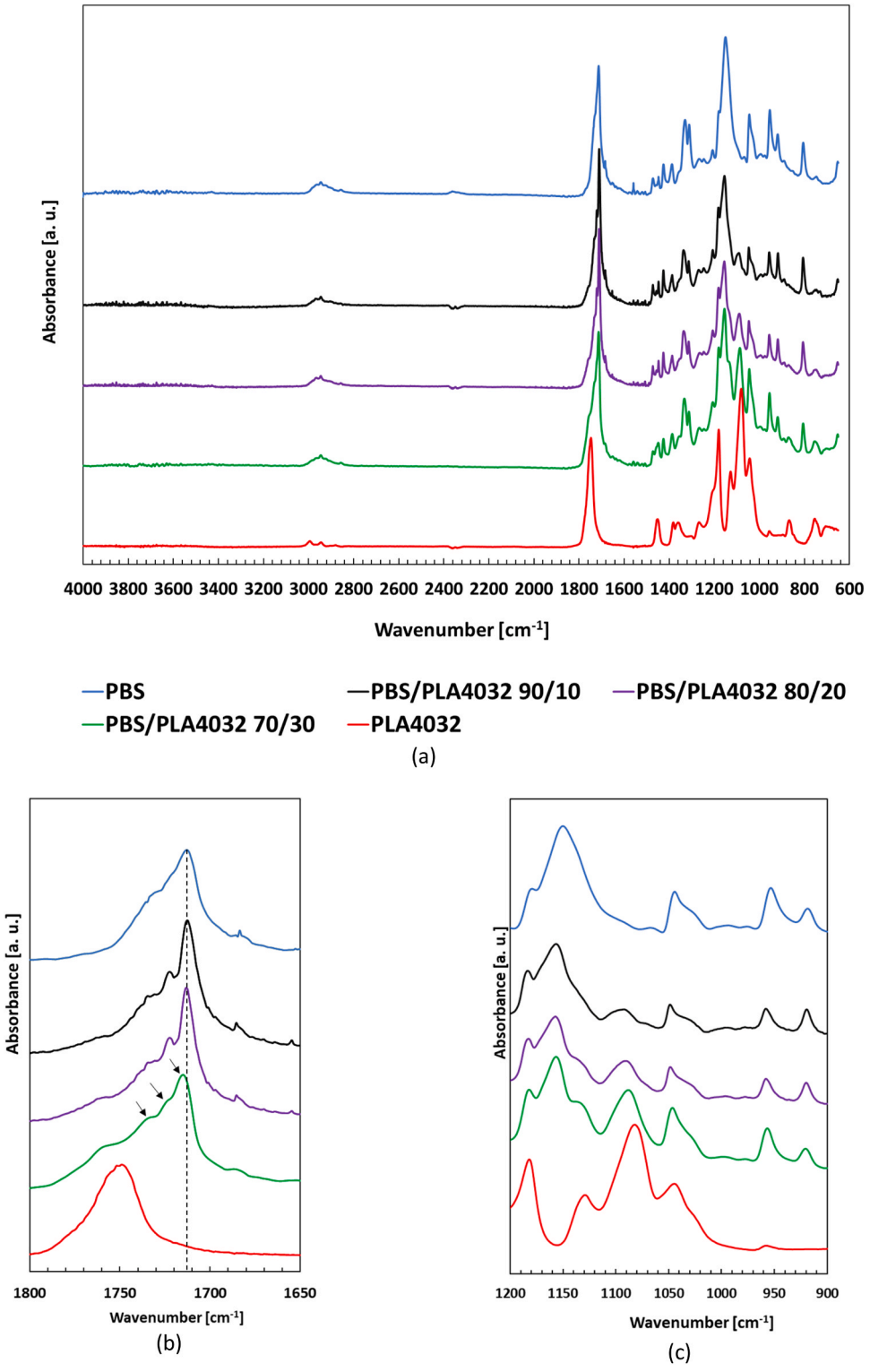

Fig. 1. ATR-FTIR spectra of the monolayer films PBS, PBS/PLA4032 90/10, PBS/PLA4032 80/20, PBS/PLA4032 70/30, PLA4032: (a) in the full x-axis scale; (b) zoom of the carbonyl bonds; (c) zoom of the C-O-C bonds.

$$W_a = 2\left(\sqrt{\gamma_O^d \gamma_I^d} + \sqrt{\gamma_O^p \gamma_I^p}\right) \quad (4)$$

In Eq. (3), γ_{SL}, γ_L and γ_S are the interfacial energy and the surface energies of the liquid and solid phases, respectively. In Eq. 4, the subscript "I" and "O" stand for the inner and outer layer surfaces, respectively, while the superscript "d" and "p" indicate the dispersive and polar components, respectively.

Hot filling tests were carried out by simulating the steps and the processing conditions occurring in real packaging lines. Pouches having 4 × 16 cm^2 size were cut and sealed from rolled stock film using heat sealer HSG-C (Brugger, Germany) with 90 °C sealing temperature, a pressure of 1 N/mm^2 (F = 650 N) and welding time equal to 1 s. Then, the pouches were filled with 40 mL of hot water at 85 °C, simulating pasteurized water-based foods, and were manually sealed with minimal headspace. Then, they were cooled in water bath at a temperature of 4 °C for 3 min and visually inspected to assess whether the seal had held up and if the film had deformations, wrinkles or folds. The bags were finally stored in the freezer at − 18 °C for two months, to check the performance of the packaging after medium-long storage at freezing conditions. Seven replicates were made for each film type.

3. Results and discussion

3.1. FTIR-ATR analysis

FTIR analysis was carried out on monolayer films to obtain information about possible interaction between polymers in the blends.

Fig. 1 displays the spectra of single layer films PBS, PLA4032 and based on PBS/PLA blends 90/10, 80/20 and 70/30. Typical absorption bands of polylactide and poly(butylene succinate) are observable in the spectra of pure films. In particular, the ATR-FTIR plot of the PBS film exhibits the principal characteristic absorptions as follows: the stretching of C-H groups at 2800–3000 cm^{-1}; the absorption peak of the carbonyl group C═O stretching vibration at 1712 cm^{-1}; the CH stretching in CH_2 in 1471–1311 cm^{-1} band; the asymmetric and symmetric C-O stretching in C-O-C at 1152 and 1044 cm^{-1}, respectively; the C-OH bending in the carboxylic group at 917 cm^{-1}. The ATR-FTIR trace of PLA4032 shows the following absorption peaks: C-H asymmetric stretching at 2991 cm^{-1}; the C═O stretching vibration of the carbonyl group at 1747 cm^{-1}; the C-H deformation in CH3 at 1451 cm^{-1}; the symmetric and asymmetric C-H deformation at 1852 and 1357 cm^{-1} respectively; the C-O stretching in C-O-C in 1180–1043 cm^{-1} band; the C-COO stretching at 867 cm-1. No new absorption bands were detectable in the spectra of the PBS/PLA4032 blends were observed, although some peak shifts were detected. In particular, as the PLA content increases, the peak of the PBS carbonyl group shifts from 1712 cm^{-1} to 1716 cm^{-1} in the PBS/PLA4032 70/30 blend; moreover, when PLA content is 30 %, three absorption bands related to the C═O stretching vibration region become clearly visible at 1735, 1725 and 1716 cm^{-1}, which are identified with the free amorphous, the rigid amorphous and the crystalline phases of PBS, respectively (Yao, Chen, & Ye, 2017). As the content of PLA in the blend increases, also the PBS peaks relative to the asymmetric and symmetric C-O stretching move from 1148 and 1043 cm^{-1} to 1155 and 1046 cm^{-1}, respectively. These shifts suggest that the polymers, while immiscible, show some interactions and a fair degree of compatibility.

Fig. 2 displays the comparison among FTIR spectra of Ecovio, PLA4060, Ecovio/PLA4060 80/20 and Ecovio/PLA4060 70/30 monolayer films. The trace of neat Ecovio shows characteristic peaks related both to PLA and PBAT. The mains for PBAT are: 2954 cm^{-1} (C-H stretching), 1711 cm^{-1} (C-O stretching), 1409 cm^{-1} (trans-CH2-plane bending), 1267 cm^{-1} (C-O symmetric stretching), 1101 cm^{-1} (C-O left-right symmetric stretching), 935 cm^{-1} (C-O stretching) and 726 cm^{-1} (CH_3 bending). The mains for PLA are: 1455 cm^{-1} (CH deformation in CH_3), 1386 cm^{-1} (C-H symmetric deformation), 1180 cm^{-1} (C-O stretching in C-O-C) and 872 cm^{-1} (C-COO stretching). In the blends only some minor changes occurred in the intensity and sharpness of the PLA peaks at 1747 cm^{-1} (C═O stretching vibration), 1180 cm^{-1} (C-O stretching) and 1044 cm^{-1} (C-O stretching), but no shifts were detectable. This indicates the realization of a physical blend, without any molecular structure mutation of the constituents.

3.2. Thermal transitions and crystallinity

DSC measurements were conducted on the monolayer films to

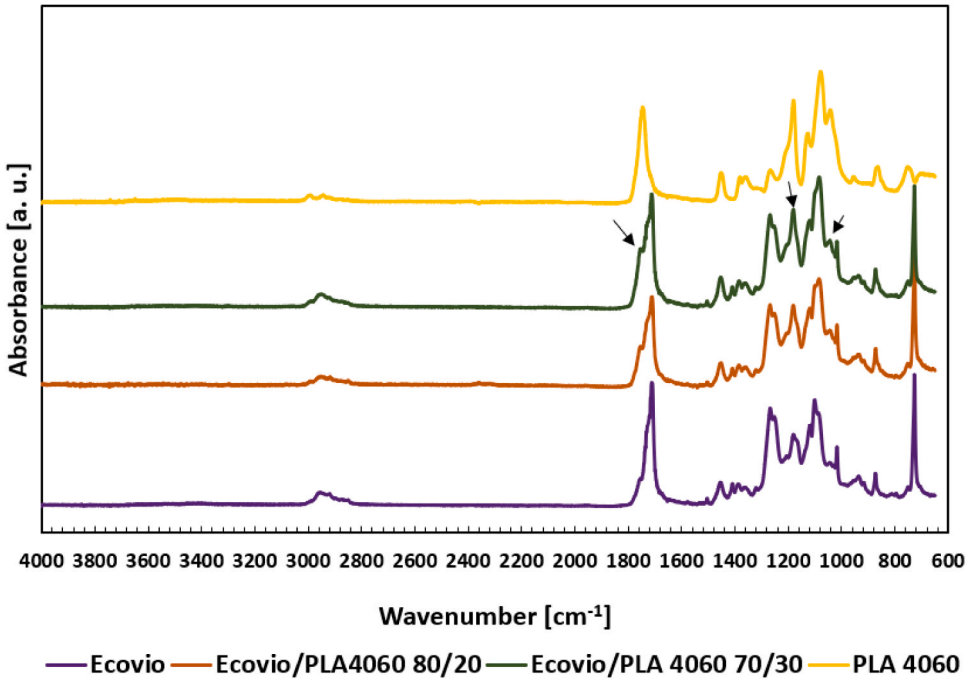

Fig. 2. ATR-FTIR spectra of the monolayer films Ecovio, Ecovio/PLA4060 80/20, Ecovio/PLA4060 70/30 and PLA4060.

evaluate their morphology, which deeply affects the mechanical behavior, barrier performance and heat resistance, and to study any potential change in the thermal behavior of polymer phases due to mixing.

Fig. 3 displays the first heating thermograms for the single layer films PBS, PLA4032 and based on PBS/PLA blends 90/10, 80/20 and 70/30, while the relative thermal parameters are displayed in Table 2.

The neat PBS thermogram shows one exothermic transition at 115 °C corresponding to melting of the crystalline fraction of the polymer, while the glass transition temperature related to its amorphous fraction could not be detected, even when scans from − 70 °C have been carried out (data not shown). However, it is known that PBS exhibits a T_g at − 32 °C, so it keeps its ductile behavior for temperatures above (Su, Kopitzky, Tolga, & Kabasci, 2019). On the other hand, PLA4032 exhibit a glass transition temperature at 65 °C, a broad cold crystallization peak in the range 90–118 °C and a melting peak at 168 °C.

All the PBS/PLA4032 blends show two exhotermic peaks at ca. 87 °C and ca. 99–102 °C, attributable to PBS and PLA, respectively, and two separate melting peaks derived from the constituent polymers; this indicates the presence of clearly separated domains belonging to the two distinct polymers, and that phase separation ensues (Ostrowska et al., 2019). However, the presence of PBS leads to a decrease of the glass transition temperature (Tg) of PLA, suggesting some limited miscibility of PBS and PLA in the amorphous phase and subsequent plasticization of PLA (Park & Im, 2002); The addition of PBS also causes a shift in the cold crystallization peak in mixtures towards lower temperatures compared to pure PLA, indicating that it increases the PLA crystallization rate. As can be seen from the themograms in Fig. 3, the cold crystallization peak of PLA overlaps with the melting peak of PBS at about 105–110 °C: this makes it difficult to determine the PLA crystallinity degree in the blends. However, as reported by Ostrowska et al. (2019), it is worth to underline that the films were extruded and then crystallized under the same conditions, so it is reasonable to suppose the same thermal records for these samples; this implies that, although there are errors in determining the crystallinity of PLA using this method, the errors are the same for each sample. Taking this into account, the results in Table 2 show an increase of PLA crystallinity degree (Xc) in the blends with respect to pure PLA, reaching the highest value for PBS/PLA4032 70/30 monolayer film (46.6 %). Similar outcomes were reported by other authors (Deng & Thomas, 2015; Ostrowska et al., 2019; Yokohara & Yamaguchi, 2008) and are ascribable to a higher mobility of the PLA chains in the presence of the PBS, with an increased ability to crystallize. The outcomes of Table 2 highlight an increase in the crystallinity degree also for the PBS phase in the blends with respect to the neat PBS film, and reaches the highest value for the PBS/PLA4032 80/20 monolayer sample (65.2 %).

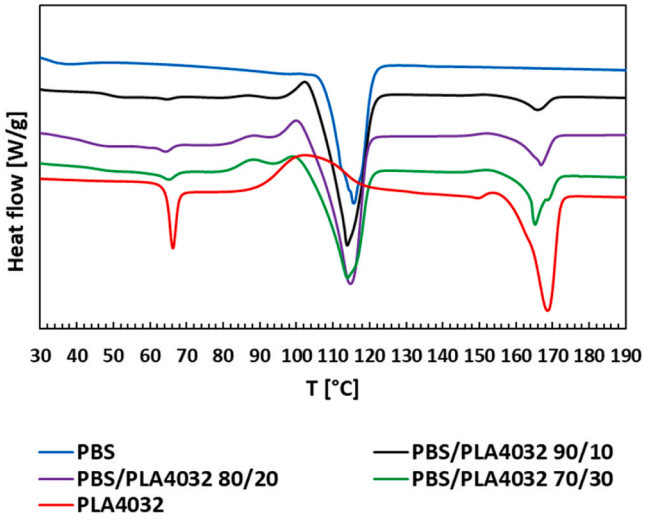

Fig. 3. DSC first heating thermograms of the monolayer films PBS, PBS/PLA4032 90/10, PBS/PLA4032 80/20, PBS/PLA4032 70/30, PLA4032.

Table 3 presents the first heating thermogram and thermal parameters for the monolayer films Ecovio, Ecovio/PLA4060 80/20, Ecovio/PLA4060 70/30 and PLA4060, respectively. All films based on Ecovio and its blends show thermal properties characteristic of the biopolymers of which it consists, i.e., PLA and PBAT. Specifically, the glass transition temperature around − 30 °C and the endothermic peaks at ca. 50 °C and 120 °C, respectively, are characteristic of PBAT, while the Tg at 60 °C and the endothermic peak at ca. 150 °C are ascribable to semicrystalline PLA within the Ecovio matrix (Pietrosanto et al., 2020). Neat PLA4060, on its side, is completely amorphous, with only the glass transition visible at ca. 60 °C, which is followed by the characteristic relaxation related to polymer ageing. No significant changes are observed in the thermal behavior of the mixtures as the PLA4060 content increases.

3.3. Optical microscopy

The bilayer coextruded films were investigated by optical microscopy in order to verify the uniformity of the layers' shape and thickness, which play a key role in the development of the overall film properties.

Fig. 4 reports the image taken on the Coex O50/I30 structure, chosen as an example. The optical microscopy analysis of the bilayer films revealed that, under the working conditions used in our study, all the coextruded films have layers with flat and well defined interfaces between the individual layers, and constant thickness along the transversal film section. The absence of interfacial gaps or debonding within the cross sectional images indicate the good interlayer adhesion achieved; the boundaries between the layers appear sharp and smooth, without interlayer mixing or diffusion and detectable interfacial defects. Moreover, as observable in Fig. 4, the calculated thicknesses of the layers by OM were fairly in accordance with the nominal ones, pointing out the good control of the layers thicknesses achieved during the co-extrusion process.

3.4. Oxygen and water vapor barrier properties

The oxygen and water vapor barrier are key constraints for materials intended for food packaging applications, as their presence could result in detrimental changes in the safety and quality of a food product. In particular, for frozen products made from juices, sauces or gravies, an adequate barrier is needed not only to oxygen, to protect the food from oxidative phenomena caused by gas permeation, but also to water vapor, to shield it from dehydration phenomena caused by moisture evaporation through the packaging walls. In order to investigate how the transport behavior is affected by the blends composition and by the multilayer layout, oxygen and water vapor permeability tests were carried out on all single layer and coextruded systems and outcomes are reported in Table 4.

Both the water vapor and oxygen permeability coefficients of the neat PBS and Ecovio monolayers are comparable to literature data reported for films based on PBS and PBAT/PLA blends, respectively (Bumbudsanpharoke, Wongphan, Promhuad, Leelaphiwat, & Harnkarnsujarit, 2022; Pietrosanto et al., 2020). As for PBS/PLA4032 blends, the addition of semicrystalline PLA results in a decrease in the oxygen permeability coefficient compared with both pure PBS and PLA4032 films. For the PBS/PLA4032 70/30 film a maximum decrease in P_{O_2} value of 47 % is obtained, compared to pure PBS. This can be reasonably associated with the increase in the crystallinity degree (Xc %) of both PBS and PLA in the blends, as evidenced by DSC analysis; specifically, the crystalline degree of PLA reaches the highest value for this sample, equal to 46.6 %. The crystals hinder the permeation of oxygen through the films by increasing the tortuosity of the gas diffusional pathway, as also evidenced by the reduction of the diffusivity coefficient as the PLA content in the mixture increases. On the other hand, PLA4032 incorporation did not substantially affect the water vapor permeability

Table 2
Thermal parameters of the monolayer films PBS, PBS/PLA4032 90/10, PBS/PLA4032 80/20, PBS/PLA4032 70/30, PLA4032, related to the first heating cycle.

Sample Film	PBS					PLA					
	T_{cc} [°C]	ΔH_{cc} [J/g]	T_m [°C]	ΔH_m [J/g]	X_C^a [%]	T_g [°C]	T_{cc} [°C]	ΔH_{cc} [J/g]	T_m [°C]	ΔH_m [J/g]	X_C^b [%]
PBS	n.d.	n.d.	115.7	57.2	52.3	-	-	-	-	-	-
PBS/PLA4032 90/10	86.5	0.7	113.8	61.2	60.9	63.4	102.2	2.6	165.7	4.4	19.2
PBS/PLA4032 80/20	87.7	0.9	114.7	58.4	65.2	63.1	99.8	2.4	165.9	8.8	34.2
PBS/PLA4032 70/30	87.7	1.7	113.8	50.4	63.1	63.7	98.9	1.1	165.2	14.2	46.6
PLA4032	-	-	-	-	-	65.3	102.5	30.9	168.5	38.3	7.9

[a] degree of crystallization of PBS in the blend calculated according to the equation $Xc = (\Delta H_m - \Delta H_{cc})/\phi i * \Delta H_m^0$, where $\Delta H_m$is the melting enthalpy of PBS, ΔH_{cc} is the cold crystallization temperature of PBS, $\Delta H_m^0 = 110.3$ J/g is the melting enthalpy of 100 % crystalline PBS and ϕi represents the relative weight fraction of PBS in the blends.
[b] degree of crystallization of PLA in the blend calculated according to the equation $Xc = (\Delta H_m - \Delta H_{cc})/\phi i * \Delta H_m^0$, where $\Delta H_m$is the melting enthalpy of PLA, ΔH_{cc} is the cold crystallization temperature of PLA, $\Delta H_m^0 = 93.7$ J/g is the melting enthalpy of 100 % crystalline PLA and ϕi represents the relative weight fraction of PLA in the blends.

Table 3
Thermal parameters of the monolayer films Ecovio, Ecovio/PLA4060 80/20, Ecovio/PLA4060 70/30 and PLA4060, related to the first heating cycle.

Sample Film	Tg_{PBAT} [°C]	Tg_{PLA} [°C]	$Tm1_{PBAT}$ [°C]	$\Delta Hm1_{PBAT}$ [J/g]	$Tm2_{PBAT}$ [°C]	$\Delta Hm2_{PBAT}$ [J/g]	Tm_{PLA} [°C]	ΔHm_{PLA} [J/g]
Ecovio	-29.6	63.4	50.4	1.2	121.3	6.4	149.6	0.2
Ecovio/PLA4060 80/20	-27.9	58.3	42.5	1.2	120.3/132.6	5.3	148.5	0.2
Ecovio/PLA4060 70/30	-28.4	59.3	43.9	0.9	116.7	3.0	148.0	0.3
PLA4060	-	60.1	-	-	-	-	-	-

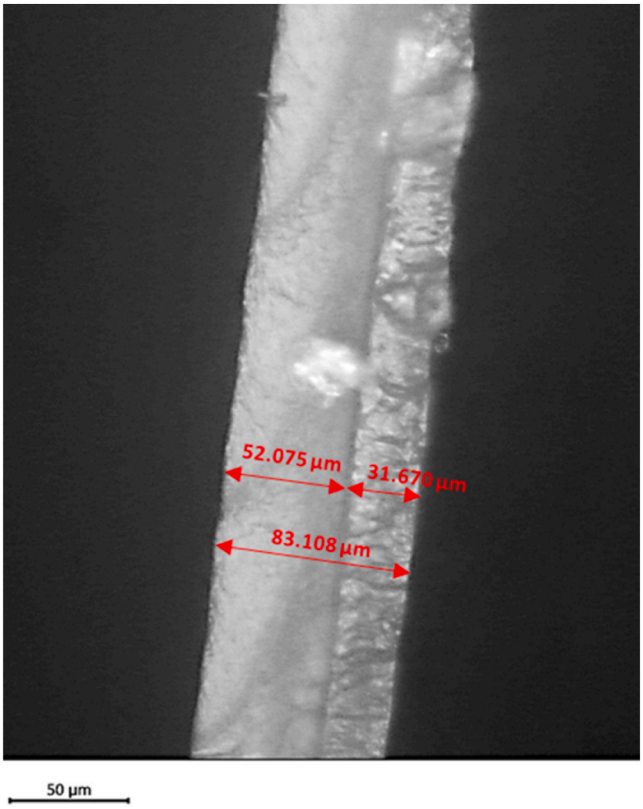

Fig. 4. Optical microscopy image of the Coex O50/I30 bilayer film (section normal to the extrusion direction), with magnification 20x).

coefficient. However, both the P_{O_2} and P_{H2O} values are in line with permeabilities reported by other authors for PBS/PLA blends having a PBS content ≥50 % (Threepopnatkul & Preedanorawut, 2022; Risse, Tighzert, Berzin, & Vergnes, 2014).

As for Ecovio/PLA4060 blends, the addition of PLA4060, although amorphous, also contributes to the reduction of the oxygen and water vapor permeability coefficients with respect to the Ecovio matrix, with a maximum decrease equal to 52 % and 16 %, respectively, for the Ecovio/PLA4060 70/30 monolayer film. This could be a consequence of the increase in PLA fraction having reduced mobility compared to PBAT, which means a lower fraction of free volume between the polymer chains. (Pietrosanto et al., 2020).

Basing on these results, the blends PBS/PLA4032 70/30 and Ecovio/PLA4060 70/30 were selected for the realization of the outer and inner layers of the bilayer films, respectively.

The oxygen and water vapor permeability coefficients obtained for the coextruded films are averaged over the P_{O_2} and P_{H2O} values of the inner and outer layer films. In particular, the P_{O_2} is weighted on the relative thicknesses, i.e. decreases by increasing the thickness of the outer layer, and increases by increasing the thickness of the inner layer. In contrast, the water vapor permeability remains substantially constant for all the multilayer films.

The oxygen permeability coefficient for the multilayer configurations was also calculated according to the Eqs. (1) and (2) mentioned above in the "Materials and methods" section, and the results are shown in Table 4 as $P_{calc\_O_2}$. As can be seen, a good agreement was found between measured and experimental oxygen permeability values, with a calculated percentage difference of less than 5 % in each case, highlighting the good control of the relative film thicknesses achieved during the coextrusion process.

The best barrier performance was obtained for Coex O50/I30 sample, exhibiting P_{O_2} and P_{H2O} values equal to 14.2 $\frac{cm^3}{m^2 d}\frac{mm}{bar}$ and 0.56 $\frac{gmm}{m^2 d}$, respectively. These values were compared with data available in the literature on biodegradable coextruded films based on Ecovio F2223/starch (Wu 2021), PLA/PLA-layered silicate/PLA (Scarfato et al., 2017), PHBV/PBAT (Cunha et al., 2016) and were found at par or up to two orders of magnitude lower.

3.5. Tensile properties at −18, 25 and 85 °C

Mechanical properties are essential because films must have sufficient mechanical strength and extensibility to ensure their integrity and sustain external stresses throughout the life cycle of the packaged food

Table 4
Measured water vapor permeability (P_{H2O}), oxygen permeability (P_{O_2}) and diffusivity (D) coefficients for all monolayer and multilayer films. Calculated oxygen permeability ($P_{calc\_O_2}$)values for multilayer films according to Eqs. (1) and (2). Percentage difference among experimental and calculated oxygen permeability values, calculated as follows: $|P_{O_2} - P_{calc\_O_2}|/[(P_{O_2} + P_{calc\_O_2})/2] \times 100$.

Sample	$P_{H2O}\left[\frac{gmm}{m^2 d}\right]$	D * 10^7 [cm^2/s]	$P_{O_2}\left[\frac{cm^3\ mm}{m^2 d\ bar}\right]$	$P_{calc\_O_2}\left[\frac{cm^3\ mm}{m^2 d\ bar}\right]$	Percentage difference [%]
Monolayer films					
PBS	0.48	1.2	21.1		
PBS/PLA4032 90/10	0.47	0.7	20.2		
PBS/PLA4032 80/20	0.47	0.6	18.0		
PBS/PLA4032 70/30	0.45	0.3	11.1		
PLA4032	1.30	0.5	32.1		
Ecovio	3.10	3.0	69.0		
Ecovio/PLA4060 80/20	2.80	0.7	35.7		
Ecovio/PLA4060 70/30	2.60	0.6	33.4		
Bilayer films					
Coex O30/I30	0.57	0.5	16.8	16.6	0.6
Coex O30/I50	0.59	0.5	18.2	19.0	4.6
Coex O50/I30	0.56	0.4	14.2	14.8	4.5

product. What is more, in-service conditions significantly affect the properties of thermoplastic polymers (Şerban, Weber, Marşavina, Silberschmidt, & Hufenbach, 2013). In order to ascertain the perspectives of the developed structures as biodegradable packaging suitable for either hot filling process and storage at room and freezing temperatures, the tensile properties of the multilayer films produced were evaluated at

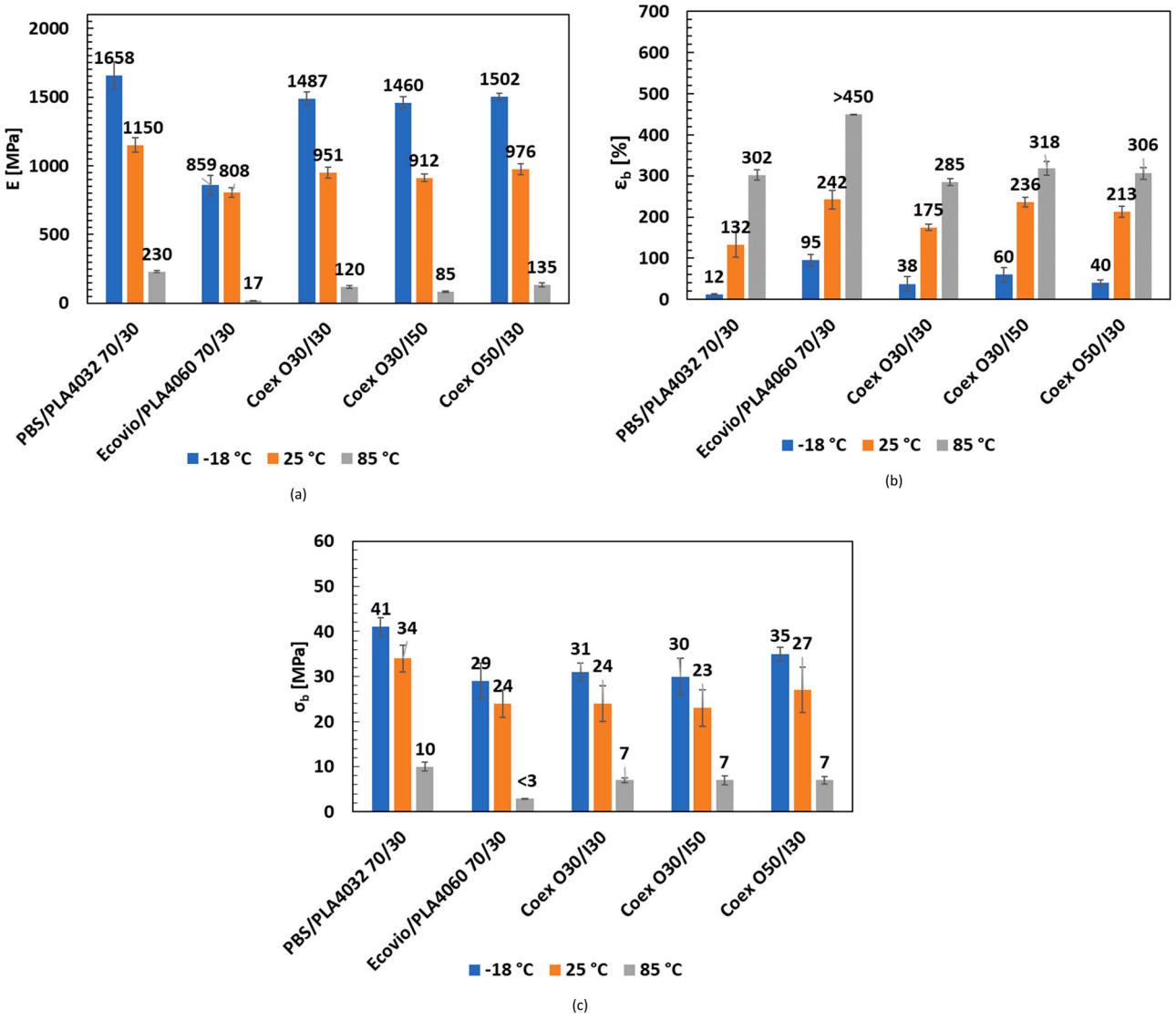

Fig. 5. Elastic modulus (E) (a), elongation at break (ε_b) (b) and tensile strength at break (σ_b) (c) for single outer (PBS/PLA4032 70/30) and inner (Ecovio/PLA4060 70/30) layers and multilayer films at −18, 25 and 85 °C.

25 °C, −18 °C and 85 °C. The results, expressed as elastic modulus E, stress at break σ_b and strain at break ε_b, are displayed in Fig. 5, and compared to those obtained for the single inner and outer layers films.

At 25 °C, the PBS/PLA4032 70/30 layer exhibits a good compromise between stiffness and ductility, with an elastic modulus equal to 1150 ± 52 MPa and a percentage of elongation at break equal to 132 ± 30 %. On the other side, the Ecovio/PLA4060 70/30 shows a very ductile behavior, with a percentage of elongation at break equal to 242 ± 22 % and tensile properties comparable to that of mixtures containing 40 % PBAT or more (Pietrosanto et al., 2020).

The mechanical properties of multilayer films are intermediate to those of individual inner and outer layers, and are to some extent influenced by the layout of the systems. In particular, the Coex O30/I50, i.e. the one with the largest thickness of the inner layer, shows the least value of elastic modulus and stress at break, whereas the ε_b value is the highest. On the contrary, the Coex O30/I50, having the largest thickness of the outer layer, shows the largest value of E and σ_b and a lower strain at break with respect to the Coex O30/I50. The Coex O30/I30 film, instead, shows an intermediate behavior in terms of E and σ_b parameters, while it has the worst performance in terms of strain at break.

The graphs of Fig. 5 displayed how the temperature decrease from 25 °C to −18 °C implied, for all the tested films, an increase in both elastic modulus and stress at break, while the elongation at break decreased. This depends on the reduction of the polymers chain flexibility and of the increase in the material stiffness due to the temperature lowering. However, this variation had a different magnitude depending on the blends' composition for the monolayers and, of course, depending on the multilayers configuration. In detail, the single outer layer stiffens more, and shows an increase in Young's modulus up to 1658 MPa (+44 % compared to E at 25 °C) while the elongation at break decreases to 12 % (- 90 % compared to ε_b at 25 °C). The single inner layer, on the other hand, retains its elastic modulus almost unchanged, with only a 6 % increase over E at 25 °C, while the elongation at break at −18 °C remains above 90 %. This may be attributable to the high mobility of the polymer chains constituting the blend, in particular of PBAT, which at −18 °C is still in the rubbery state, that make ductility less sensitive to decreasing temperature. Notably, other authors have shown similar behavior for PBAT/PLA blends with PBAT content above 40 %, for which the failure mode remains ductile up to −25 °C (Pietrosanto et al., 2020).

At −18 °C, conversely, the failure mode of the PBS/PLA4032 70/30 outer layer changes from ductile at room temperature to brittle, and this can be reasonably attributable to the high crystalline content of both PBS and PLA4032, which makes it more difficult for the chains to slide over each other, resulting in a less ductile material. At −18 °C for all three multilayer films there is an increase in elastic modulus up to ca. 1500 MPa, and an increase in strength at break in the 30–35 MPa range. However, the presence of the inner layer of Ecovio/PLA4060 contributes to guarantee an elongation at break of more than 38 % in all cases and, for the Coex O30/I50 sample (i.e., the film with the thickest outer layer), of 60 %.

At a temperature of 85 °C, as expectable, a significant collapse in E and σ_b and an increase in ε_b values are observed for all the films analyzed. At high temperatures, indeed, the polymer chains show increased flexibility and are prone to warping in the direction of the applied stress.

The Ecovio/PLA4060 70/30 film shows the most consistent decrease in elastic modulus (from 808 MPa at 25 °C to 17 MPa at 85 °C) and σ_b (from 24 MPa at 25 °C to <3 MPa at 85 °C), while the elongation at break is above 450 %. These results can be interpreted in light of the thermal transitions of the polymers constituting the blend. As underlined by the DSC results, the temperature of 85 °C is above the Tg of both PBAT and amorphous PLA4060, and above the melting temperature of the crystalline fraction of the butylene adipate phase (Gan, Kuwabara, Yamamoto, Abe, & Doi, 2004). Therefore, the amorphous fraction of both polymers is in the rubbery state, while the crystalline fraction of PBAT is partially melted. Specifically, as the temperature increases, there is a breakdown of those secondary physical bonds between the polymer chains in the amorphous phase (i.e., Van der Waals dipole-dipole interactions) that limit the molecular movements and identify the initial stiffness. Therefore, the significant elongation at 85 °C is attributable to the higher mobility due to the breakage of tie molecules in the amorphous phase as well as to the loss of crystalline fraction (Amjadi & Fatemi, 2020; Hocker, Kim, Schniepp, & Kranbuehl, 2018).

Contrariwise, for the PBS/PLA4032 70/30 film, the temperature of 85 °C between Tg and Tm of both PBS of PLA4032; therefore, the amorphous fraction is in the rubbery state while the high crystalline fraction of both polymers remains intact. This leads to higher Young's modulus (i.e. 203 MPa) and ultimate tensile strength (i.e. 10 MPa) and lower strain at break (i.e. 302 %) with respect to Ecovio/PLA4060 70/30.

It is also valuable to point out that PBS shows a heat delfection temperature (HDT) of 88 °C or higher, while PBAT shows an HDT of 46 °C (Muthuraj, Misra, & Mohanty, 2015). Besides, a high crystalline content generally increases the HDT: in the literature, some authors have observed that, between 37 % and 42 % of crystallinity, heat deflection temperature of PLA increased from approx. 60 °C to above 120 °C (Péter, Litauszki, & Kmetty, 2021).

In the multilayer films, the presence of the PBS/PLA outer layer helps to mitigate the loss of performance of the Ecovio/PLA inner layer, so the elastic modulus is held in the range between 85 MPa (for the Coex O30/I50 film) and 135 MPa (for the Coex O50/I30 film), the average ultimate tensile strength is 7 MPa for all samples, and the elongation at break is within 285 % (for the Coex O30/I30 film) and 318 % (for the Coex O30/I50 film). Out of all, the film with the thickest outer layer thickness, i.e. Coex O50/I30, retains the highest stiffness, suggesting to be the best candidate as packaging for hot filled products.

3.6. DMA analysis

Thermomechanical properties of the PBS/PLA4032 70/30, Ecovio/PLA4060 70/30 monolayers and of the bilayer film Coex O50/I30 were investigated by DMA, in order to provide better insights into the viscoelastic behavior of the samples, enabling a more comprehensive understanding of their mechanical performance and of the interfacial interactions between the layers of the coextruded systems. The storage modulus (E′) and loss tangent curves (Tan δ) as a function of temperature are shown in Fig. 6(a) and (b), respectively.

As observable in Fig. 6(a), the storage moduli of all the films exhibited a decrease with increasing temperature, indicating a decrease in the films' stiffness as they underwent softening transitions. In particular, for all the curves it can be observed a sharp drop of the storage modulus around − 30 °C, which is ascribable to the glass transition temperature of both the PBS (Zhang, He, & Yin, 2019) and PBAT (Zhang, He, Lin et al., 2019; Ko et al., 2021) phases. Another sharp drop in the elastic modulus in observable around 60 °C, corresponding to the glass transition temperature of the PLA (Ko et al., 2021). The comparison revealed that the storage values, determined by DMA curves, agreed fairly well with those determined from tensile tests at the three temperatures investigated (Fig. 5(a)).

The Tan δ curves ((Fig. 6(b)) for all the samples investigated displayed only one distinctive peak at around 60 °C, related to the PLA. For all the films investigated, the damping factor is always less than 1, indicating that the materials analyzed are predominantly elastic in nature; however, PBS/PLA4032 70/30 shows the lowest intensity of the Tan δ peak, indicating the highest elastic behavior and lowest segmental motions of the polymer matrix during the transition. The Tan δ curve of the Coex O50/I30 is intermediate with respect to the ones of the single layer films. It is worth to notice the peak broadening and asymmetry in the bilayer film, as well as the shift towards lower temperatures with respect to both PBS/PLA4032 70/30 and Ecovio/PLA4060 70/30. This

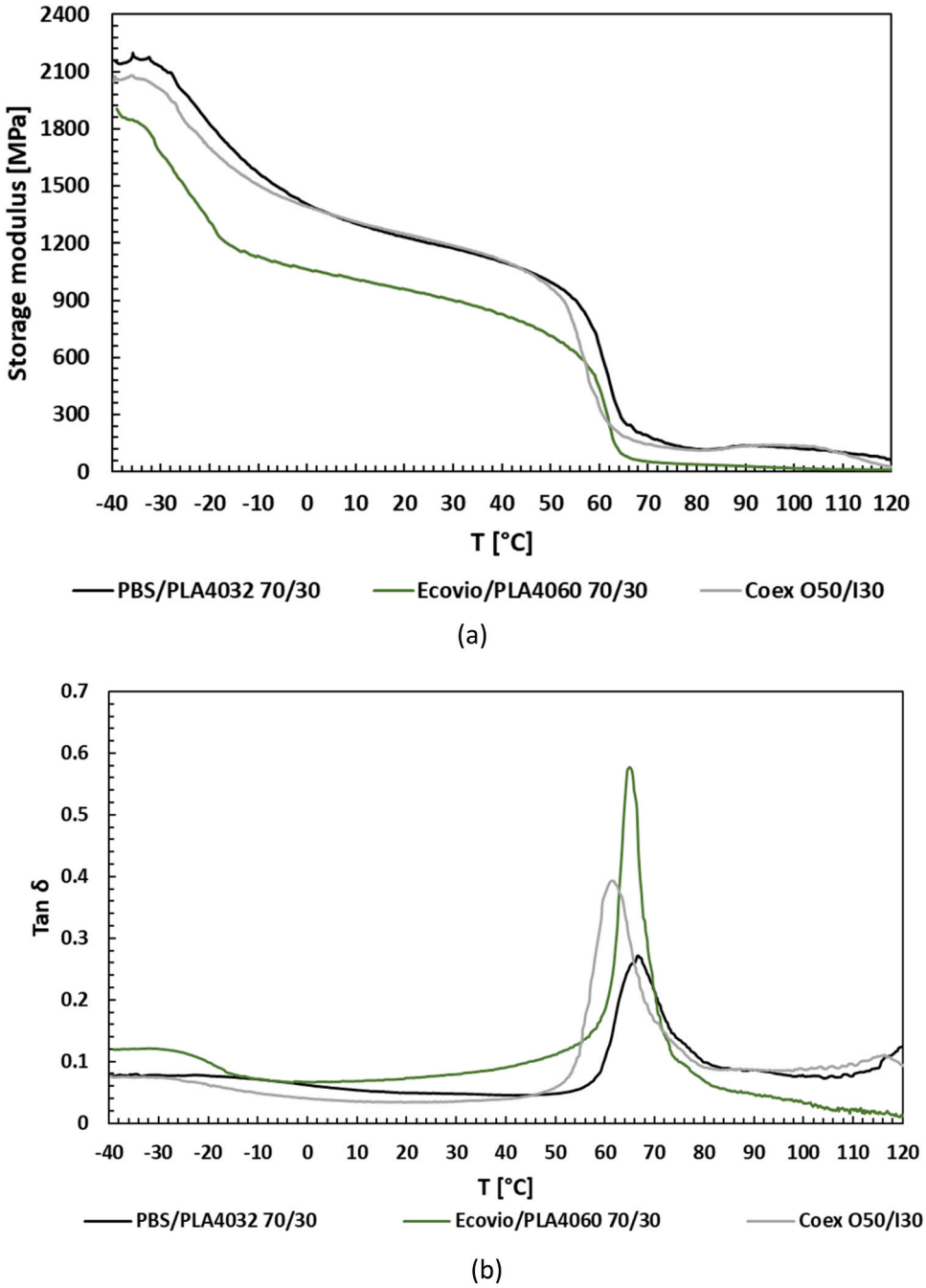

Fig. 6. Storage modulus (a) and tan δ curves (b) of the single outer (PBS/PLA4032 70/30) and inner (Ecovio/PLA4060 70/30) layers and bilayer film Coex O50/I30.

behavior suggests a variation of relaxation times associated with the two layers, possibly arising from interfacial interactions and interdiffusion of polymer chains across the layers.

3.7. Overall migration tests

In order to investigate the migration behavior of the coextruded films in contact with foods, overall migration tests were carried out on the inner layer Ecovio/PLA4060 70/30 of the Coex O30/I50 sample (i.e., the one with the largest thickness of inner layer) taken as representative of all the coextruded films. 3 % acetic acid, 20 % ethanol and 50 % ethanol in distilled water (simulants B, C and D1) were selected according to the Regulation (EU) No 10/2011 as the set of food simulants to measure the suitability of packages in contact with unfiltered drinks, cloudy drinks and juices (e.g. fruit juice popsicles). The test conditions (10 days at 40 °C) were chosen as contact simulation for any long-term storage at room temperature or below, including heating up to 100 °C for up to 15 min; therefore, these conditions are suitable both for storage in ambient and in frozen conditions, as well as for hot filling of liquid

Table 5
Overall migration in 3 % acetic acid (simulant B), 20 % ethanol (simulant C), and 50 % ethanol (simulant D1) from the inner layer Ecovio/PLA4060 70/30 of the Coex O30/I50 sample, taken as representative of all the coextruded films. Contact conditions: 10 days at 40 °C.

Food simulant	Overall migration value [mg/dm^2]
3 % acetic acid	0.73 ± 0.2
20 % ethanol	0.65 ± 0.2
50 % ethanol	0.86 ± 0.3

foods.

Table 5 reports the average results of the overall migration tests, performed in the three selected simulants. Low overall migration levels, in the range of analytical tolerances, were measured in all the cases. Taking into consideration the uncertainties of the analytical method, no significant differences were detected between the samples, and in all the cases the overall migration values remained below the migration limits (10 mg/dm^2) established by the European Union Legislation for the contact of plastic materials with food (European Commission, 2011).

3.8. Evaluation of hot seal strength

When developing films for food packaging applications, the quality of heat seals is of paramount importance. In particular, the evaluation of the hot tack strength, i.e. the maximum weight that the seal is able to withstand without breaking, is crucial to assess the suitability of the packaging materials for applications in form-fill-seal lines. Fig. 7(a) shows the hot tack curves for the for Ecovio based monolayers and for all coextruded multilayer films.

The monolayer films based on PBS were not sealable in the whole range of temperatures investigated, whereas neat Ecovio was sealable only in a narrow range of temperatures between 90 °C and 100 °C, with a maximum hot tack strength equal to 275 g/15 mm at 95 °C. The addition of 20 % and 30 % PLA4060 in the Ecovio matrix allows both to extend the sealable temperature range, with a decrease of the hot-tack initiation temperature of 10 °C, and to increase the maximum hot tack strength up to 500 and 600 g/15 mm at 90 °C, respectively. This effect is attributable to the good sealing properties of amorphous PLA, which improves the chain mobility and diffusion in the blends; in particular, the greater the diffusion, the easier will be the molecular penetration across the interface, implying stronger bonds at lower temperatures (Apicella & Carlucci, 2022; Tabasi, Najarzadeh, & Ajji, 2015).

The multilayer configurations show a significant increase of the hot tack strength, which is in any case maximum at 90 °C. In particular, both films Coex O30/I50 and Coex O50/I30, having a total thickness of 80 μm, exhibit a maximum hot tack strength equal to 1325 g/15 mm, with an increase of 120 % with respect to the Ecovio/PLA4060 70/30 monolayer. For the Coex O30/I30 film, having a total thickness of 60 μm, these values are equal to 1275 g/15 mm and 112 %, respectively. These results indicate that both the inner and outer layers of the films were involved in the melting and re-solidification process, and that the maximum sealing strength depends more on the total thickness of the coextruded films than on the relative thicknesses of the outer/inner layers.

According to the ASTM F 1921–98, the failure mode of the sealed test strips was visually determined at all the tested temperatures and for all the tested films, and described in accordance with the classification reported within the standard. Fig. 7(b) illustrates the pictures and sketches of the failure modes of the sealed test strips at 80, 90 and 100 °C for the Coex O50/I30 multilayer film, taken as example.

It is worth noting that, for all the samples analyzed, peel adhesive failure of the seal occurs at 80 °C, whereas at temperatures equal or higher than 85 °C the material breaks at the seal edge. It is also important to highlight that the seal strength of coextruded multilayers is comparable or lower than the values typical of seal layers based on polyolefins (Morris, 2017). Moreover, the developed films exhibit a maximum seal strength at temperatures below 100 °C, therefore, they are suitable for applications in high-speed packaging lines where the hot seal undergoes a certain pressure, such as in vertical form-fill-seal processes (Bamps et al., 2022).

3.9. Wettability, surface energies and work of adhesion measurements

Contact angle measurements have been carried out to calculate films' surface energies and to evaluate the goodness of the interlayer adhesion of the multilayer systems.

Static contact angles for the inner (Ecovio/PLA4060 70/30) and outer (PBS/PLA4032 70/30) layers surfaces of the coextruded films in water (CA_W) and diiodomethane (CA_{DM}) are presented in Table 6. Representative images of the water and diiodomethane drops on each films analysed surface were also provided in Fig. 8. Taking into account small variations due to the experimental method, the values obtained were similar for all the multilayer films investigated. Using these angles, the surface free energies (γ_S), comprising of polar (γ_s^p) and dispersive (γ_s^d) components, and the polarity (P_s) were estimated following the Owens–Wendt approach (Table 6). The results of the surface energies allowed to calculated adhesion and interfacial energy at the interface of the multilayer films Coex O30/I30, Coex O30/I50 and Coex O50/I30, as reported in Table 7.

The contact angle values for the Ecovio/PLA4060 70/30 and PBS/PLA4032 70/30 surfaces are in line with those reported in the literature for the neat biodegradable polymers of which the blends are composed (Scaffaro et al., 2020; Marturano et al., 2019; Hu, Su, Li, & Wang, 2018; Wang L.F., 2016). Low polarity values were obtained, confirming the inherent hydrophobicity of the polymers.

What is worth to noting is that both the inner and outer layer exhibit comparable values of polar (γ_s^p) and dispersive (γ_s^d) components of the surface free energy. According to the literature, the amount of polar and dispersion bonds deeply affects the extent of the adhesion force between two layers, which is maximum when the ratio between γ_s^p and γ_s^d values is close to unity. As further evidence, all three multilayer films show very high values of the work of adhesion, while the interfacial energy calculation returns values close to zero for the Coex O30/I30 sample, and even negative for Coex O30/I50 and Coex O50/I30 films. According to the work of adhesion theory, indeed, a high work of adhesion entails not only high surface energies of either the coextruded layers, but also minimum interfacial energy values, indicating high interfacial compatibility (Ebnesajjad & Landrock, 2015). Therefore, the obtained results underline the good interlayer adhesion achieved for bilayer films after the coextrusion process, denoting adequate adhesion for industrial-scale polymer assembly (Apicella & Carlucci, 2022).

3.10. Evaluation of suitability for hot filling tests and effect on oxygen permeability

In light of the results discussed above, the bilayer systems were also subjected to hot filling tests by simulating the steps and the processing conditions occurring in real packaging lines described in the "Experimental" section. Fig. 9 depicts the images of the pouches made by Coex O30/I30, Coex O30/I50 and Coex O50/I30 after hot filling process at 85 °C, filled (a, b, c) and empty (d, e, f) and after hot filling process and frozen storage at −18 °C for two months (g, h, i).

Preliminary tests were carried out on Ecovio/PLA4060 70/30 monolayer, which withstanded to a maximum hot filling temperature equal to 65 °C. Above that limit, the films becomes very tacky, and the bottom side seam breaks completely. As for the coextruded films, on the other hand, the addition of the outer layer based on PBS/PLA blends ensures in all cases the films to withstand the maximum temperature of 85 °C, without any breakage of the bottom side seam (Fig. 9a-f). Nonetheless, the Coex O30/I30 film shows slightly more shrinkage on the surface of the sachet and, in particular, at the sealing joint. This is observable in detail when the bag is filled with water both at room temperature (Fig. 9(a)) and at −18 °C (Fig. 9(c)). Conversely, the Coex O50/I30 and Coex O30/I50 samples exhibit, in the same conditions, a more uniform surface (Fig. 9(b) and (c) and Fig. 9(h) and (i), respectively). Likewise, the storage at −18 °C emphasizes that both samples possess sufficient ductility to withstand the increase in volume of frozen water without buckling or breaking.

In order to investigate possible changes in the barrier properties of the bilayer structures due to hot filling process, oxygen permeation measurements were also carried out on the Coex O30/I30, Coex O30/I50 and Coex O50/I30 film samples after subjecting them to hot filling

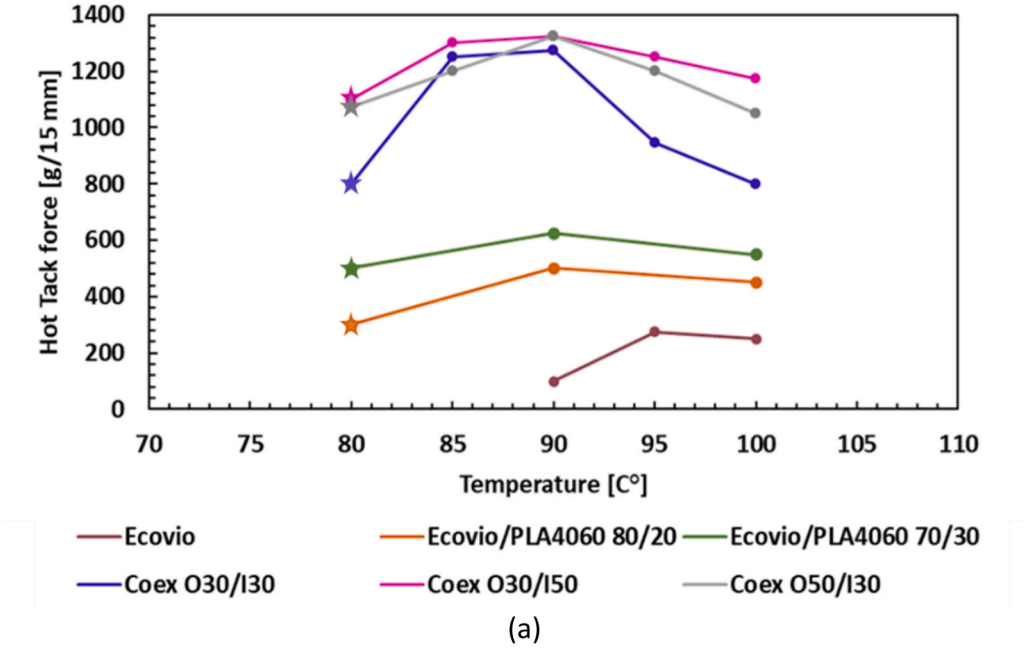

(a)

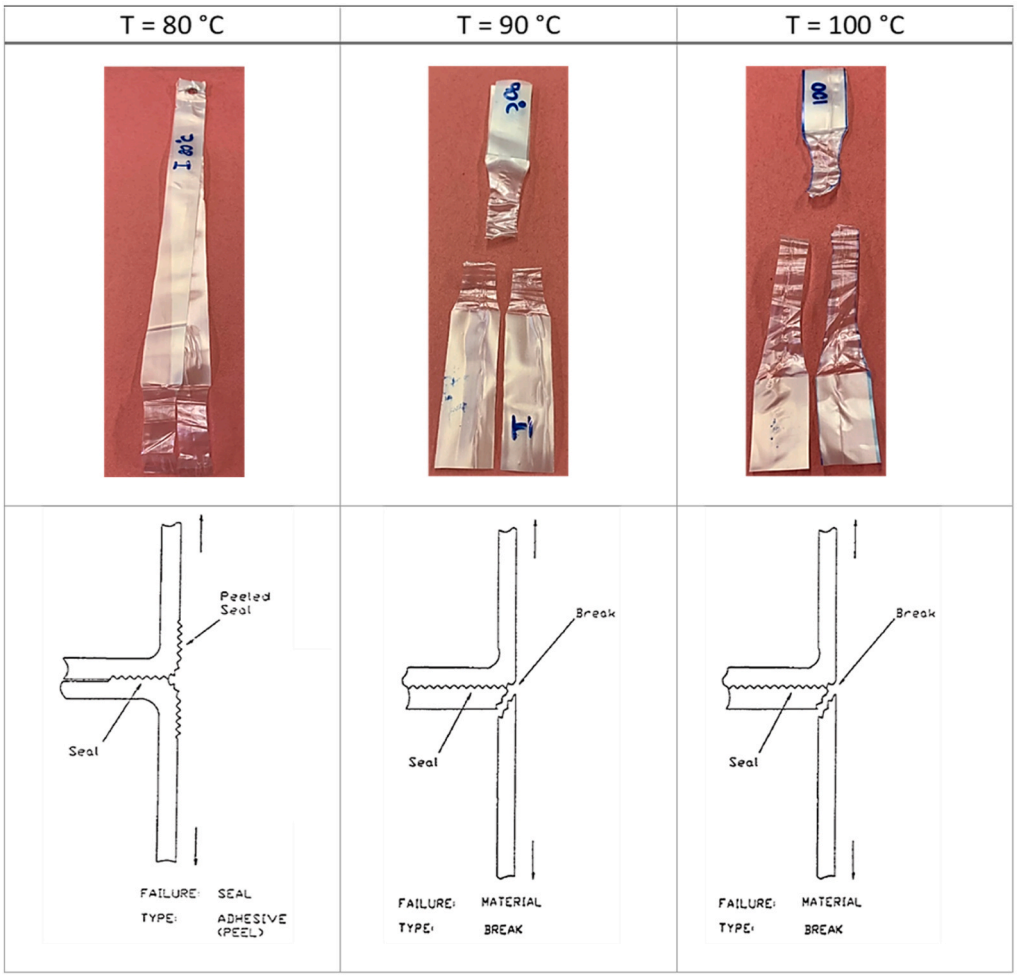

(b)

Fig. 7. (a) Hot tack curves for Ecovio, Ecovio/PLA4060 80/20 and Ecovio/PLA4060 70/30 monolayers and for all multilayer films. Stars represent the experimental points at which peel adhesive failure of the seal occurs, while the dots represent the points at which material breaks at the seal edge; (b) pictures and sketches of the failure modes of the sealed test strips at 80, 90 and 100 °C for the Coex O50/I30 multilayer film, taken as example.

Table 6
Static contact angles for the inner (Ecovio/PLA4060 70/30) and outer (PBS/PLA4032 70/30) layers surfaces of the coextruded films in water (CA_W) and diiodomethane (CA_{DM}). Surface free energies (γ_S) comprising of polar (γ_s^p) and dispersive (γ_s^d) components and polarity (P_s), following the Owens–Wendt approach.

Films analysed surface	CA_W [°]	CA_{DM} [°]	γ_s^p [mN/m]	γ_s^d [mN/m]	P_s [-]	γ_S [mN/m]
O: PBS/PLA4032 70/30	66.9 ± 0.6	40.4 ± 1.5	10.0	37.2	0.21	47.2
I: Ecovio/PLA4060 70/30	66.8 ± 1.2	39.0 ± 2.5	9.7	38.0	0.22	47.7

tests. As a matter of fact, thermal processing may result in changes in gas and vapor barrier properties affecting the packaging performance. For this reason, knowledge of the extent of variations in barrier properties is critical (Sonar, Al-Ghamdi, Marti, Tang, & Sablani, 2020). The results highlighted that, for all the coextruded structures, the oxygen permeability coefficient increased after the thermal treatment. In particular, the P_{O2} values of Coex O30/I30, Coex O30/I50 and Coex O50/I30 increased from unprocessed values of 16.8, 18.2 and 14.2 $\frac{cm^3 \quad mm}{m^2 d \quad bar}$ to after processing values of 22.7, 24.6 and 20.1 $\frac{cm^3 \quad mm}{m^2 d \quad bar}$, respectively. As also reported by other authors, the decrease in the barrier properties of biodegradable polyester-based films may be attributable to some partial hydrolysis of the macromolecules along with some plasticization of polymeric chains, leading to higher chain mobility and increased free volume (Galotto, Ulloa, Guarda, Gavara, & Miltz, 2009; Bhunia et al., 2016). However, it is worth noting that the relative variation in oxygen permeability of the coextruded films, which remained within 35 % in all cases, is comparable to that reported in the literature for commercial PET/PE films subjected to thermal pasteurization treatment at 72 ± 0.5 °C for 13–15 min; it was also demonstrated that, within this range, changes in oxygen and water vapor permeability have little effect on the quality of in-package thermal pasteurized, high-moisture products stored under refrigeration conditions (Sonar et al., 2020).

4. Conclusions

In this study, coextruded blown films based on tailor-made PBS/PLA and Ecovio/PLA biodegradable blends were realized by lab-scale co-extrusion plant, with the aim to design a novel structure suitable for hot-filling and frozen food packaging applications.

The infrared spectroscopy carried out on PBS/PLA4032 monolayer films revealed that PBS and PLA4032, although immiscible, have some interactions. In particular, the presence of PBS raised the crystallinity degree of PLA4032 from 8 % for pure PLA, to 46.6 % of PBS/PLA4032 70/30 blend. Thanks to the high crystalline fraction, this sample exhibited the lowest oxygen permeability and retained the highest Young's modulus (i.e. 203 MPa) and ultimate tensile strength (i.e. 10 MPa) at 85 °C. The stiffness of the system, however, caused the elongation at break to reduce at 12 % at −18 °C.

In the Ecovio/PLA4060 blends, on the other hand, the addition of PLA4060 in the Ecovio matrix allowed to decrease the hot tack initiation

Table 7
Calculated work of adhesion (W_α) and interfacial energy (γ_{sl}) of the coextruded films Coex O30/I30, Coex O30/I50 and Coex O50/I30.

Films interface	W_α [mN/m]	γ_{sl} [mN/m]
Coex O30/I30	95.0	0.005
Coex O30/I50	92.3	-0.620
Coex O50/I30	95.7	-0.366

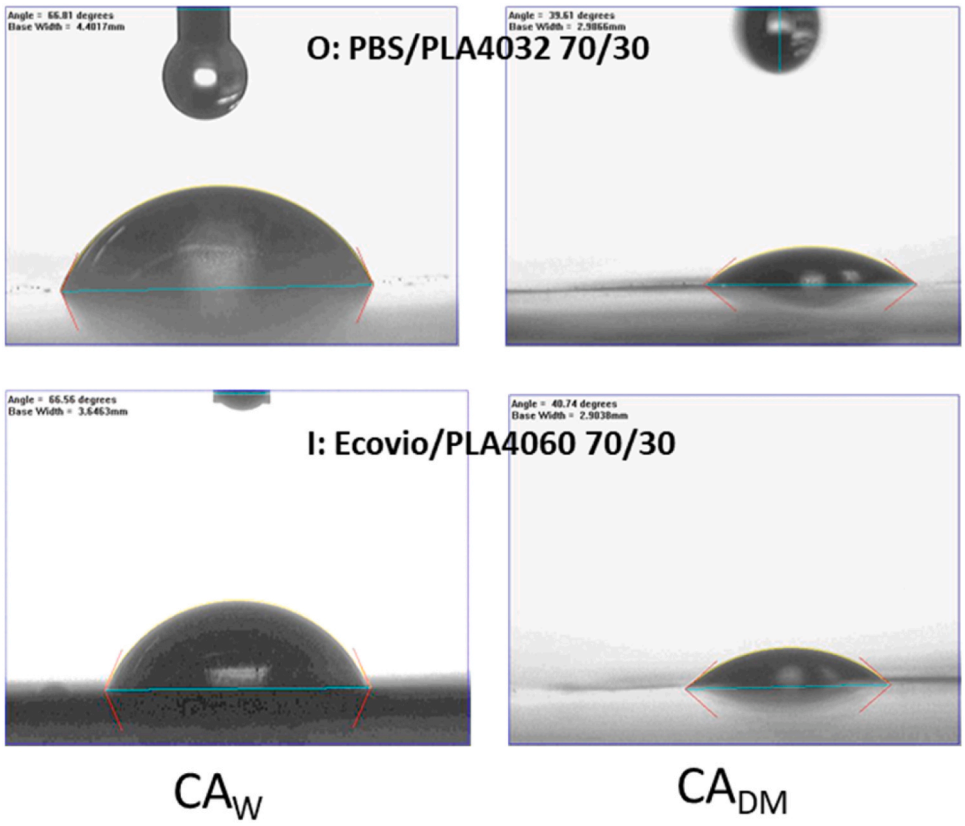

Fig. 8. Representative images of the water and diiodomethane drops on each films analysed surface.

Fig. 9. Images of the pouches made by bilayer films Coex O30/I30, Coex O30/I50 and Coex O50/I30 after hot filling process at 85 °C, filled (a, b, c), and empty (d, e, f) and after hot filling process and frozen storage at −18 °C for two months (g, h, i).

temperature from 90° to 80°C, and to increase the hot tack strength. In particular, the Ecovio/PLA4060 70/30 film was the one with the maximum hot tack strength, while it exhibited an elongation at break still higher than 90 % at −18 °C. On the other hand, it showed very poor thermal resistance, as underlined by tensile tests at 85 °C.

On the bases of the aforementioned considerations, PBS/PLA4060 70/30 and Ecovio/PLA4060 70/30 were selected as optimal blends for the realization of the outer and inner layers of the bilayer films, respectively. The coextrusion process allowed a good control of the relative layer thicknesses, and all the produced systems exhibited high interlayer adhesion and interfacial compatibility, as also suggested by DMA analysis exhibiting a shift towards lower temperatures of Tg of bilayer Coex O50/I30 with respect to the inner and outer single layer films.

The functional properties of the bilayer structures were found intermediate with respect to those of individual inert and outer layers, and were influenced by the layout of the systems. In particular, the barrier properties and the stiffness increased by increasing the thickness of the outer layer, whereas the ductility increased by increasing the thickness of the inner layer, at all test temperatures.

The maximum sealing strength, on its side, depended on the total thickness of the coextruded films rather than on the relative outer/inner layer thickness, reaching the highest value, equal to 1325 g/15 mm, at 90 °C for both Coex O50/I30 and Coex O30/I50 samples.

To directly highlight the perspectives for the produced multilayer films for the target application, their mechanical properties at −18, 25 and 85 °C were evaluated. The results of the tensile tests show that, out of all, the Coex O50/I30 film retains the best balance between stiffness and ductility over such a wide range of operating temperatures (i.e. from −18° to 85°C), and is therefore the most suitable for both freezing and hot filling applications: at 85 °C, in fact, it has an elastic modulus of 135 MPa, a tensile strength of 7 MPa and an elongation at break of 306 %, while at −18 °C it retains an elongation at break equal to 40 %. What is more, the film still possesses satisfactory O_2 barrier properties after a hot filling test simulating conditions similar to those occurring on a real packaging line. Finally, the overall migration values endorsed its suitability for food contact applications, involving both hot filling and long-term frozen food storage.

CRediT authorship contribution statement

Annalisa Apicella: Conceptualization, Methodology, Investigation, Data curation. Writing – original draft. **Paola Scarfato:** Conceptualization, Methodology, Supervision, Data curation, Validation, Writing – review & editing. **Loredana Incarnato:** Conceptualization, Supervision, Writing – review & editing, Funding acquisition.

Declaration of Competing Interest

The authors declare that they have no known competing financial interests or personal relationships that could have appeared to influence the work reported in this paper.

Data Availability

Data will be made available on request.

References

Adegoke, G.O. (2004). Understanding Food Microbiology (2nd ed.). Alleluia Ventures, Ibadan, Nigeria.

Ahmed, J., Mulla, M. Z., Al-Zuwayed, S. A., Joseph, A., & Auras, R. (2022). Morphological, barrier, thermal, and rheological properties of high-pressure treated co-extruded polylactide films and the suitability for food packaging. *Food Packaging and Shelf Life, 22*, Article 100812. https://doi.org/10.1016/j.fpsl.2022.100812

Aliotta, L., Seggiani, M., Lazzeri, A., Gigante, V., & Cinelli, P. (2022). A brief review of poly (Butylene Succinate) (PBS) and its main copolymers: synthesis, blends, composites, biodegradability, and applications. *Polymers, 14*, 844. https://doi.org/10.3390/polym14040844

Amjadi, M., & Fatemi, A. (2020). Tensile behavior of high-density polyethylene including the effects of processing technique, thickness, temperature, and strain rate. *Polymers, 12*, 1857. https://doi.org/10.3390/polym12091857

Andrade, M. S., Ishikawa, O. H., Costa, R. S., Seixas, M. V. S., Rodrigues, R. C. L. B., & Moura, E. A. B. (2022). Development of sustainable food packaging material based on biodegradable polymer reinforced with cellulose nanocrystals. *Food Packaging and Shelf Life, 31*, Article 100807. https://doi.org/10.1016/j.fpsl.2021.100807

Apicella, A., Barbato, A., Garofalo, E., Incarnato, L., & Scarfato, P. (2022). Effect of PVOH/PLA + wax coatings on physical and functional properties of biodegradable food packaging films. *Polymers, 14*, 935. https://doi.org/10.3390/polym14050935

Apicella, A., Carlucci, E., Leneveu-Jenvrin, C., Remize, F., & Scarfato, P. (2022). Active coated films to decrease browning of minimally processed banana fruit. *Macromolecular Symposia, 405*, 2100256. https://doi.org/10.1002/masy.202100256

Apicella, A., Scarfato, P., Di Maio, L., & Incarnato, L. (2018). Oxygen absorption data of multilayer oxygen scavenger-polyester films with different layouts. *Data in Briefing, 19*, 1530–1536. https://doi.org/10.1016/j.dib.2018.06.024

Bamps, B., Guimaraes, R. M. M., Duijsters, G., Hermans, D., Vanminsel, J., Vervoort, E., Buntinx, M., & Peeters, R. (2022). Characterizing mechanical, heat seal, and gas barrier performance of biodegradable films to determine food packaging applications. *Polymers, 14*, 2569. https://doi.org/10.3390/polym14132569

Bhunia, K., Zhang, H., Liu, F., Rasco, B., Tang, J., & Sablani, S. S. (2016). Morphological changes in multilayer polymeric films induced after microwave-assisted pasteurization. *Innovative Food Science & Emerging Technologies, 38*, 124–130. https://doi.org/10.1016/j.ifset.2016.09.024

Boufarguine, M., Guinault, A., Miquelard-Garnier, G., & Sollogoub, C. (2013). PLA/PHBV films with improved mechanical and gas barrier properties. *Macromolecular Materials and Engineering, 298*, 1065–1073. https://doi.org/10.1002/mame.201200285

Bumbudsanpharoke, N., Wongphan, P., Promhuad, K., Leelaphiwat, P., & Harnkarnsujarit, N. (2022). Morphology and permeability of bio-based poly (butylene adipate-co-terephthalate) (PBAT), poly(butylene succinate) (PBS) and linear low-density polyethylene (LLDPE) blend films control shelf-life of packaged bread. *Food Control, 132*, Article 108541. https://doi.org/10.1016/j.foodcont.2021.108541

Chen, G. X., & Yoon, J. S. (2005). Thermal stability of poly(l-lactide)/poly(butylene succinate)/clay nanocomposites. *Polymer Degradation and Stability, 88*, 206–212. https://doi.org/10.1016/j.polymdegradstab.2004.06.005

Chen, Q., Auras, R., Corredig, M., Kirkensgaard, J. J. K., Mamakhel, A., & Uysal-Unalan, I. (2022). New opportunities for sustainable bioplastic development: Tailorable polymorphic and three-phase crystallization of stereocomplex polylactide by layered double hydroxide. *International Journal of Biological Macromolecules, 222*, 1101–1109. https://doi.org/10.1016/j.ijbiomac.2022.09.205

Cunha, M., Fernandes, B., Covas, J. A., Vicente, A. A., & Hilliou, L. (2016). Film blowing of PHBV blends and PHBV-based multilayers for the production of biodegradable packages. *Journal of Applied Polymer Science, 133*, 42165. https://doi.org/10.1002/app.42165

Deng, Y., & Thomas, N. L. (2015). Blending poly(butylene succinate) with poly(lactic acid): Ductility and phase inversion effects. *European Polymer Journal, 71*, 534–546. https://doi.org/10.1016/j.eurpolymj.2015.08.029

Ebnesajjad, S., & Landrock, A.H. (2015). Adhesives Technology Handbook (3rd ed.), William Andrew Publishing.

European Bioplastics. (2022). Bioplastics market data. Retrieved from ⟨https://www.european-bioplastics.org/market/⟩. Accessed January 24, 2023.

European Commission. (2011). Commission regulation (EU) No 10/2011 of 14 January 2011 on plastic materials and articles intended to come into contact with food. *Official Journal of European Community, 12*, 1–89, 2011; L.

Facchi, D. P., Souza, P. R., Almeida, V. C., Bonafé, E. G., & Martins, A. F. (2021). Optimizing the Ecovio® and Ecovio®/zein solution parameters to achieve electrospinnability and provide thin fibers. *Journal of Molecular Liquids, 321*, Article 114476. https://doi.org/10.1016/j.molliq.2020.114476

Galotto, M. J., Ulloa, P. A., Guarda, A., Gavara, R., & Miltz, J. (2009). Effect of high pressure food processing on the physical properties of synthetic and biopolymer films. *Journal of Food Science, 74*, E304–E311. https://doi.org/10.1111/j.1750-3841.2009.01212.x

Gan, Z., Kuwabara, K., Yamamoto, M., Abe, H., & Doi, Y. (2004). Solid-state structures and thermal properties of aliphatic-aromatic poly(-butylene adipate-co-butylene terephthalate) copolyesters. *Polymer Degradation and Stability, 83*, 289–300. https://doi.org/10.1016/S0141-3910(03)00274-X

Gigante, V., Canesi, I., Cinelli, P., Coltelli, M. B., & Lazzeri, A. (2019). Rubber Toughening of Polylactic Acid (PLA) with Poly(butylene adipate-coterephthalate) (PBAT): Mechanical properties, fracture mechanics and analysis of ductile-to-brittle behavior while varying temperature and test speed. *European Polymer Journal, 115*, 125–137. https://doi.org/10.1016/j.eurpolymj.2019.03.015

Gigante, V., Coltelli, M. B., Vannozzi, A., Panariello, L., Fusco, A., Trombi, L., Donnarumma, G., Danti, S., & Lazzeri, A. (2019). Flat die extruded biocompatible poly(lactic acid) (PLA)/Poly(butylene succinate) (PBS) based films. *Polymers, 11*, 1857. https://doi.org/10.3390/polym11111857

Grzebieniarz, W., Biswas, D., Roy, S., & Jamróz, E. (2023). Advances in biopolymer-based multi-layer film preparations and food packaging applications. *Food Packaging and Shelf Life, 35*, Article 101033. https://doi.org/10.1016/j.fpsl.2023.101033

Hocker, S. J. A., Kim, W. T., Schniepp, H. C., & Kranbuehl, D. E. (2018). Polymer crystallinity and the ductile to brittle transition. *Polymer, 158*, 72–76. https://doi.org/10.1016/j.polymer.2018.10.031

Homklin, R., & Hongsriphan, N. (2013). Mechanical and thermal properties of PLA/PBS co-continuous blends adding nucleating agent. *Energy Procedia, 34*, 871–879. https://doi.org/10.1016/j.egypro.2013.06.824

Hongdilokkul, P., Keeratipinit, K., Chawthai, S., Hararak, B., Seadan, M., & Suttiruengwong, S. (2015). A study on properties of PLA/PBAT from blown film process. *IOP Conference Series: Materials Science and Engineering, 87*, Article 012112. https://doi.org/10.1088/1757-899X/87/1/012112

Hu, X., Su, T., Li, P., & Wang, Z. (2018). Blending modification of PBS/PLA and its enzymatic degradation. *Polymer Bulletin, 75*, 533–546. https://doi.org/10.1007/s00289-017-2054-7

Jeong, S., Lee, H. G., Cho, C. H., & Yoo, S. (2020). Characterization of multi-functional, biodegradable sodium metabisulfite-incorporated films based on polycarprolactone for active food packaging applications. *Food Packaging and Shelf Life, 25*, Article 100512. https://doi.org/10.1016/j.fpsl.2020.100512

Johnson, M. L. (2018). The effect of hot fill and hold processing on the performance of multilayer packaging films. *All Theses*, 2852.

Ko, E., Kim, T., Ahn, J., Park, S., Pak, S., Kim, M., & Kim, H. (2021). Synergic Effect of HNT/oMMT Bi-filler system for the mechanical enhancement of PLA/PBAT film. *Fibers and Polymers, 22*, 2163–2169. https://doi.org/10.1007/s12221-021-1006-x

Kumar, R., Verma, A., Shome, A., Sinha, R., Sinha, S., Jha, P. K., Kumar, R., Kumar, P., Shubham, Das, S., Sharma, P., & Vara Prasad, P. V. (2021). Impacts of plastic pollution on ecosystem services, sustainable development goals, and need to focus on circular economy and policy interventions. *Sustainability, 2021*(13), 9963. https://doi.org/10.3390/su13179963

Leneveu-Jenvrin, C., Apicella, A., Bradley, K., Meile, J., Chillet, M., Scarfato, P., Incarnato, L., & Remize, F. (2021). Effects of maturity level, steam treatment, or active packaging to maintain the quality of minimally processed mango (Mangifera

indica cv. José). *Journal of Food Processing and Preservation, 45*, Article e15600. https://doi.org/10.1111/jfpp.15600
Li, C., Jiang, T., Wang, J., Peng, S., Wu, H., Shen, J., Guo, S., Zhang, X., & Harkin-Jones, E. (2018). Enhancing the oxygen-barrier properties of polylactide by tailoring the arrangement of crystalline lamellae. *ACS Sustainable Chemistry & Engineering, 6*, 6247–6255. https://doi.org/10.1021/acssuschemeng.8b00026
Li, J., Qin, X., Liu, X., Li, J., & Zhong, J. (2022). Enhanced mechanical, barrier and antioxidant properties of rice protein/sodium alginate-based films by incorporating cellulose nanocrystals and rosemary extract. *Food Packaging and Shelf Life, 34*, Article 101000. https://doi.org/10.1016/j.fpsl.2022.101000
Li, X., Ai, X., Pan, H., Yang, J., Gao, G., Zhang, H., Yang, H., & Dong, L. (2018). The morphological, mechanical, rheological, and thermal properties of PLA/PBAT blown films with chain extender. *Polymers for Advanced Technologies, 29*, 1706–1717. https://doi.org/10.1002/pat.4274
Marturano, V., Bizzarro, V., Ambrogi, V., Cutignano, A., Tommonaro, G., Abbamondi, G. R., Giamberini, M., Tylkowski, B., Carfagna, C., & Cerruti, P. (2019). Light-responsive nanocapsule-coated polymer films for antimicrobial active packaging. *Polymers, 11*, 68. https://doi.org/10.3390/polym11010068
Messin, T., Marais, S., Follain, N., Guinault, A., Gaucher, V., Delpouve, N., & Sollogoub, C. (2020). Biodegradable PLA/PBS multinanolayer membrane with enhanced barrier performances. *Journal of Membrane Science, 598*, Article 117777. https://doi.org/10.1016/j.memsci.2019.117777
Mohr, L. C., Capelezzo, A. P., Baretta, C. R. D. M., Martins, M. A. P. M., Fiori, M. A., & Mello, J. M. M. (2019). Titanium dioxide nanoparticles applied as ultraviolet radiation blocker in the polylactic acid bidegradable polymer. *Polymer Testing, 77*, Article 105867.
Morris, B. A. (2017). The science and technology of flexible packaging. *Multilayer films from resin and process to end use (1st ed.)*. William Andrew Publishing.
Muthuraj, R., Misra, M., & Mohanty, A. K. (2015). Binary blends of poly(butylene adipate-co-terephthalate) and poly(butylene succinate): A new matrix for biocomposites applications. *AIP Conference Proceedings, 1664*, Article 150009. https://doi.org/10.1063/1.4918505
Ostrowska, J., Sadurski, W., Paluch, M., Tyński, P., & Bogusz, J. (2019). The effect of poly(butylene succinate) content on the structure and thermal and mechanical properties of its blends with polylactide. *Polymer International, 68*, 1271–1279. https://doi.org/10.1002/pi.5814
Ouahioune, L. A., Wrona, M., Becerril, R., Salafranca, J., Nerín, C., & Djenane, D. (2022). Ceratonia siliqua L. kibbles, seeds and leaves as a source of volatile bioactive compounds for antioxidant food biopackaging applications. *Food Packaging and Shelf Life, 31*, Article 100764. https://doi.org/10.1016/j.fpsl.2021.100764
Owens, D. K., & Wendt, R. C. (1969). Estimation of the surface free energy of polymers. *Journal of Applied Polymer Science, 13*, 1741–1747. https://doi.org/10.1002/app.1969.070130815
Park, J. W., & Im, S. S. (2002). Phase behavior and morphology in blends of poly(L-lactic acid) and poly(butylene succinate. *Journal of Applied Polymer Science, 86*, 647–655. https://doi.org/10.1002/app.10923
Péter, T., Litauszki, K., & Kmetty, A. (2021). Improving the heat deflection temperature of poly(lactic acid) foams by annealing. *Polymer Degradation and Stability, 190*, Article 109646.
Pietrosanto, A., Apicella, A., Scarfato, P., Incarnato, L., & Di Maio, L. (2022). Development of novel blown shrink films from poly(lactide)/poly(butylene-adipate-co-terephthalate) blends for sustainable food packaging applications. *Polymers, 14*, 2759. https://doi.org/10.3390/polym14142759
Pietrosanto, A., Scarfato, P., Di Maio, L., Nobile, M. R., & Incarnato, L. (2020). Evaluation of the suitability of poly(lactide)/poly(butylene-adipate-co-terephthalate) blown films for chilled and frozen food packaging applications. *Polymers*, *12*. https://doi.org/10.3390/POLYM12040804
Piscopo, A., Zappia, A., De Bruno, A., Pozzo, S., Limbo, S., Piergiovanni, L., & Poiana, M. (2019). Use of biodegradable materials as alternative packaging of typical Calabrian Provola cheese. *Food Packaging and Shelf Life, 21*, Article 100351. https://doi.org/10.1016/j.fpsl.2019.100351
Qiu, T. Y., Song, M., & Zhao, L. G. (2016). Testing, characterization and modelling of mechanical behaviour of poly (lactic-acid) and poly (butylene succinate) blends. *Mechanics of Advanced Materials and Modern Processes, 2*(7), 2016. https://doi.org/10.1186/s40759-016-0014-9
Rahman, S. (2011). Handbook of food process design (1st ed.). Wiley-Blackwell. Oxford; Hoboken, N.J:.
Riechers, M., Fanini, L., Apicella, A., Galván, C. B., Blondel, E., Espiña, B., Kefer, S., Keroullé, T., Klun, K., Pereira, T. R., Ronchi, F., Ruiz Rodríguez, P., Sardon, H., Viana Silva, A., Stulgis, M., & Ibarra-Gonzalez, N. (2021). Plastics in our ocean as transdisciplinary challenge. *Marine Pollution Bulletin, 164*, Article 112051. https://doi.org/10.1016/j.marpolbul.2021.112051
Risse, S., Tighzert, L., Berzin, F., & Vergnes, B. (2014). Microstructure, rheological behavior, and properties of poly(lactic acid)/poly(butylene succinate)/organoclay nanocomposites. *Journal of Applied Polymer Science, 131*, 40364. https://doi.org/10.1002/app.40364
Scaffaro, R., Maio, A., Gulino, E. F., Di Salvo, C., & Arcarisi, A. (2020). Bilayer biodegradable films prepared by co-extrusion film blowing: Mechanical performance, release kinetics of an antimicrobial agent and hydrolytic degradation. *Composites Part A: Applied Science and Manufacturing, 132*, Article 105836. https://doi.org/10.1016/j.compositesa.2020.105836
Scarfato, P., Di Maio, L., Milana, M. R., Giamberardini, S., Denaro, M., & Incarnato, L. (2017). Performance properties, lactic acid specific migration and swelling by simulant of biodegradable poly(lactic acid)/nanoclay multilayer films for food packaging. *Food Additives & Contaminants: Part A, 34,*, 1730–1742. https://doi.org/10.1080/19440049.2017.1321786
Şerban, D. A., Weber, G., Marşavina, L., Silberschmidt, V. V., & Hufenbach, W. (2013). Tensile properties of semi-crystalline thermoplastic polymers: Effects of temperature and strain rates. *Polymer Testing, 32*, 413–425. https://doi.org/10.1016/j.polymertesting.2012.12.002
Signori, F., Boggioni, A., Righetti, M. C., Rondán, C. E., Bronco, S., & Ciardelli, F. (2015). Evidences of transesterification, chain branching and cross-linking in a biopolyester commercial blend upon reaction with dicumyl peroxide in the melt. *Macromolecular Materials and Engineering, 300*, 153–160. https://doi.org/10.1002/mame.201400187
Sonar, C. R., Al-Ghamdi, S., Marti, F., Tang, J., & Sablani, S. S. (2020). Performance evaluation of biobased/biodegradable films for in-package thermal pasteurization. *Innovative Food Science & Emerging Technologies, 66*, Article 102485. https://doi.org/10.1016/j.ifset.2020.102485
Sonar, C. R., Tang, J., & Sablani, S. S. (2022). Polymer packaging for in-pack thermal pasteurization technologies. In P. Juliano, R. Buckow, M. H. Nguyen, K. Knoerzer, & J. Sellahewa (Eds.), *Food engineering innovations across the food supply chain* (pp. 307–322). Academic Press.
Su, S., Duhme, M., & Kopitzky, R. (2020). Uncompatibilized PBAT/PLA blends: Manufacturability, miscibility and properties. *Materials, 13*, 4897. https://doi.org/10.3390/ma13214897
Su, S., Kopitzky, R., Tolga, S., & Kabasci, S. (2019). Polylactide (PLA) and its blends with poly(butylene succinate) (PBS): A brief review. *Polymers, 11*, 1193. https://doi.org/10.3390/polym11071193
Tabasi, R. Y., Najarzadeh, Z., & Ajji, A. (2015). Development of high performance sealable films based on biodegradable/compostable blends. *Industrial Crops and Products, 72*, 206–213.
Thellen, C., Cheney, S., & Ratto, J. A. (2013). Melt processing and characterization of polyvinyl alcohol and polyhydroxyalkanoate multilayer films. *Journal of Applied Polymer Science, 127*, 2314–2324. https://doi.org/10.1002/app.37850
Threepopnatkul, P., & Preedanorawut, R. (2022). Poly(lactic acid) and polybutylene succinate films incorporated with modified zeolite. *Materials Today: Proceedings, 65*, 2309–2314.
Vorawongsagul, S., Pratumpong, P., & Pechyen, C. (2021). Preparation and foaming behavior of poly (lactic acid)/poly (butylene succinate)/cellulose fiber composite for hot cups packaging application. *Food Packaging and Shelf Life, 27*, Article 100608. https://doi.org/10.1016/j.fpsl.2020.100608
Wang, L. F., Rhim, J. W., & Hong, S. I. (2016). Preparation of poly(lactide)/poly(butylene adipate-co-terephthalate) blend films using a solvent casting method and their food packaging application. *LWT - Food Science and Technology, 68*, 454–461. https://doi.org/10.1016/j.lwt.2015.12.062
Wang, R., Wang, S., Zhang, Y., Wan, C., & Ma, P. (2009). Toughening modification of PLLA/PBS blends via in situ compatibilization. *Polymer Engineering and Science, 49*, 26–33. https://doi.org/10.1002/pen.21210
Wang, X., Peng, S., Chen, H., Yu, X., & Zhao, X. (2019). Mechanical properties, rheological behaviors, and phase morphologies of high-toughness PLA/PBAT blends by in-situ reactive compatibilization. *Composites Part B: Engineering, 173*, Article 107028. https://doi.org/10.1016/j.compositesb.2019.107028
Wang, Y. P., Xiao, Y. J., Duan, J., Yang, J. H., Wang, Y., & Zhang, C. L. (2016). Accelerated hydrolytic degradation of poly(lactic acid) achieved by adding poly (butylene succinate. *Polymer Bulletin, 73*, 1067–1083. https://doi.org/10.1007/s00289-015-1535-9
Yao, S. F., Chen, X. T., & Ye, H. M. (2017). Investigation of structure and crystallization behavior of poly(butylene succinate) by fourier transform infrared spectroscopy. *Journal of Physical Chemistry B, 121*, 9476–9485. https://doi.org/10.1021/acs.jpcb.7b07954
Yokohara, T., & Yamaguchi, M. (2008). Structure and properties for biomass-based polyester blends of PLA and PBS. *European Polymer Journal, 44*, 677–685. https://doi.org/10.1016/j.eurpolymj.2008.01.008
Zhang, S., He, Y., Lin, Z., Li, J., & Jiang, G. (2019). Effects of tartaric acid contents on phase homogeneity, morphology and properties of poly (butyleneadipate-co-terephthalate)/thermoplastic starch bio-composities. *Polymer Testing, 76*, 385–395. https://doi.org/10.1016/j.polymertesting.2019.04.005
Zhang, S., He, Y., Yin, Y., & Jiang, G. (2019). Fabrication of innovative thermoplastic starch bio-elastomer to achieve high toughness poly(butylene succinate) composites. *Carbohydrate Polymers, 206*, 827–836. https://doi.org/10.1016/j.carbpol.2018.11.036
Zonder, L., McCarthy, S., Rios, F., Ophir, A., & Kenig, S. (2014). Viscosity ratio and interfacial tension as carbon nanotubes distributing factors in melt-mixed blends of polyamide 12 and high-density polyethylene. *Advances in Polymer Technology*, *33*. https://doi.org/10.1002/adv.21427